JOURNAL OF GEOPHYSICAL RESEARCH, VOL. 114, B01408, doi:10.1029/2008JB005679, 2009

Interseismic uplift rates for western Oregon and along-strike variation in locking on the Cascadia subduction zone

Reed J. Burgette,[1] Ray J. Weldon II,[1] and David A. Schmidt[1]

Received 7 March 2008; revised 12 September 2008; accepted 13 October 2008; published 27 January 2009.

[1] We quantify the spatial pattern of uplift rate in western Oregon and northernmost California using tidal and leveling records to better understand the pattern of interseismic locking on the Cascadia subduction zone. We extend relative sea level time series of the six primary NOAA tide gauges to include all observations from 1925 to 2006. Previously unidentified bench mark instability biases portions of tidal records by $\leq$1.6 mm a^{-1} before correction. We determine precise relative uplift rates at the six tidal sites with an adjustment that includes rates of differenced time series as additional constraints. Our analysis of National Geodetic Survey leveling data between tide gauges corrects errors in 1941 leveling, and 184 secondary ties double the number of highest quality uplift rate estimates. Relative uplift rates from leveling are adjusted to the tidal rates, accounting for uncertainties in both data types. Tidal and leveling uplift rates agree within error for all but one of the coastal segments, where we infer systematic leveling error affects the 1988 line. Uplift rates are made absolute using an interval and location-specific geocentric sea level rise rate of 2.3 $\pm$ 0.2 mm a^{-1}. Total propagated one sigma errors for the absolute uplift rates of bench marks are $\sim$0.4 mm a^{-1}. Along-strike changes in uplift rate near 45°N and 42.8°N require two distinct changes in locking depth, as inferred from elastic dislocation modeling. The along-strike changes in locking on this portion of the Cascadia subduction zone interface correlate to the western and southern extent of the mafic Siletzia block in the fore arc.

Citation: Burgette, R. J., R. J. Weldon II, and D. A. Schmidt (2009), Interseismic uplift rates for western Oregon and along-strike variation in locking on the Cascadia subduction zone, *J. Geophys. Res.*, *114*, B01408, doi:10.1029/2008JB005679.

1. Introduction

[2] The Cascadia subduction zone poses the greatest single source of seismic hazard to the northwestern United States and southwestern Canada. To accurately quantify this hazard, information regarding the frequency of past earthquake recurrence, the along-strike rupture length, and the downdip extent of coseismic rupture is needed to constrain the potential seismic moment release of future events. Although there have been no great earthquakes on the Cascadia megathrust during the European-American historical period, numerous lines of evidence record repeated earthquakes rupturing the majority of the plate boundary [*Clague*, 1997]. The most recent earthquake occurred 26 January 1700, based on radiocarbon dating and dendrochronology of subsidence of the Cascadia coast, and historical records of tsunami arrival in Japan [*Nelson et al.*, 1995; *Satake et al.*, 1996; *Jacoby et al.*, 1997; *Yamaguchi et al.*, 1997]. Modeling of the tsunami source suggests the $M_w \sim 9.0$ event in 1700 ruptured the entire 1100 km length of the Cascadia subduction zone [*Satake et al.*, 2003]. Equal numbers of Holocene turbidite deposits in offshore channels along the Cascadia margin suggest that past earthquakes have similarly ruptured the entire length of the megathrust [*Goldfinger et al.*, 2003]. However, onshore paleoseismic records indicate that some of the previous earthquakes ruptured only part of the subduction fault along strike [*Nelson et al.*, 2006]. Likewise, there is still uncertainty regarding the downdip limit of rupture [*Petersen et al.*, 2002; *Satake et al.*, 2003]. The best estimates of where the plate interface is locked and accumulating elastic strain come from geodetic studies. Here we seek to better characterize the crustal vertical velocity field for the Oregon portion of the Cascadia margin (Figure 1) and refine the estimated extent of interplate coupling.

[3] Numerous geodetic studies of crustal deformation along the Cascadia margin have been performed over the past three decades. In the first analyses of vertical deformation from leveling and sea level observations, eastward tilting was interpreted as resulting from aseismic subduction [*Ando and Balazs*, 1979; *Reilinger and Adams*, 1982]. Observation of convergence-parallel horizontal contraction in western Washington coupled with the vertical deformation led *Savage et al.* [1981] to conclude that the subduction zone was locked and accumulating elastic strain. This interpretation has prevailed with the collection and analysis of many more geodetic and geologic data [e.g., *Holdahl et al.*, 1989; *Savage et al.*, 1991]. Longer periods of observation at Cascadia tide gauges and the 1987–1988 National Geodetic Survey (NGS) releveling campaign in the Pacific Northwest allowed

[1]Department of Geological Sciences, University of Oregon, Eugene, Oregon, USA.

0148-0227/09/2008JB005679$09.00

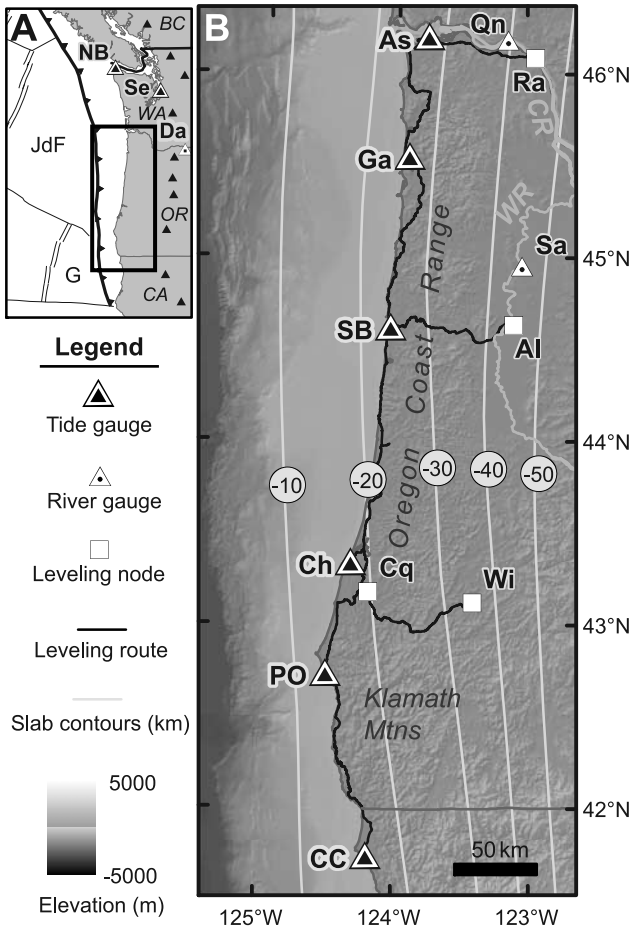

Figure 1. (a) Cascadia region, showing locations of subducting oceanic Juan de Fuca (JdF) and Gorda (G) plates. Barbed line shows the seafloor trace of the Cascadia subduction zone megathrust. Solid triangles are arc volcanoes. Heavy box shows location of Figure 1b. Tide and river gauges used in our analysis that lie outside of Figure 1b are NB, Neah Bay; Se, Seattle; and Da, The Dalles. (b) Location of tidal and leveling data from Oregon and northernmost California used in this study. Tidal sites: CC, Crescent City; PO, Port Orford; Ch, Charleston (Coos Bay); SB, South Beach (Newport); Ga, Garibaldi; As, Astoria. Leveling nodes: Cq, Coquille; Wi, Winston; Al, Albany; Ra, Rainier. Major rivers: WR, Willamette River (flows through Willamette Valley); CR, Columbia River. River gauges: Sa, Salem; Qn, Quincy.

Mitchell et al. [1994] to spatially extend and increase the precision of the vertical velocity field for the U.S. portion of the Cascadia margin. On the basis of the pattern of the uplift rates, they inferred significant along-strike variation in width and depth of the locked portion of the subduction interface. *Verdonck* [1995] used three-dimensional (3-D) elastic dislocation modeling of the *Mitchell et al.* [1994] data set for the southern section of the subduction zone to infer an isolated locked patch offshore of Reedsport, Oregon, and extending south. Using a series of trench-perpendicular two-dimensional (2-D) elastic dislocation models, *Hyndman and Wang* [1995] constrained locking using vertical deformation data from Vancouver Island to northern California. Subsequent 3-D elastic dislocation and viscoelastic models of the Cascadia subduction zone gave similar results to the locking pattern derived from the 2-D models [*Flück et al.*, 1997; *Wang et al.*, 2001]. These studies concluded that the downdip limits of the locked and transition zones run subparallel to depth contours on the slab, following modeled 350°C and 450°C isotherms, respectively.

[4] More recent studies of locking along the Cascadia subduction zone have used horizontal GPS velocities as the primary input for resolving the extent of locking on the subduction interface [*McCaffrey et al.*, 2000; *Murray and Lisowski*, 2000; *Savage et al.*, 2000; *Svarc et al.*, 2002; *Wang et al.*, 2003; *Verdonck*, 2005; *McCaffrey et al.*, 2007; *Wang*, 2007]. The increasingly high precision of horizontal GPS velocities and standardized procedures for quantifying the associated uncertainty have made these measurements more attractive for modeling. Locking patterns inferred from the horizontal data predict interseismic uplift rates that poorly match previously published estimates of vertical velocity at many locations. The historical nature of the vertical data and discrepancies between previous analyses have led modelers to downplay the importance of the vertical constraints for determining subduction zone locking [*Wang et al.*, 2003; *Wang*, 2007]. However, particularly in southern Cascadia, the dominant signal in the horizontal velocity field is rotation of the fore arc relative to stable North America [e.g., *Savage et al.*, 2000; *McCaffrey et al.*, 2007]. As the horizontal velocity field is produced by both subduction zone strain accumulation and secular motion of the fore arc, one must make additional assumptions to separate the two effects.

[5] The primary signal in the vertical velocity field of coastal Cascadia is from strain accumulation associated with subduction. Previous studies of vertical deformation have removed globally modeled predictions of uplift rate in response to postglacial isostatic adjustment [*Savage et al.*, 1991; *Hyndman and Wang*, 1995]. However, more recent local studies of the postglacial response in Cascadia have concluded that a weak upper mantle results in negligible rates of contemporary crustal velocity [*James et al.*, 2000; *Clague and James*, 2002]. As deformation from the interseismic subduction process is the primary signal in the vertical data, uplift rates from the Cascadia fore arc provide a direct indicator of the extent of locking on the plate interface. The predicted horizontal velocity field from a subduction model constrained with vertical deformation rates offers an independent means to assess horizontal rotation and other deformation of the upper plate [e.g., *Miller et al.*, 2001].

[6] The small number of permanent GPS receivers with sufficiently long records and the lower signal-to-noise ratio along the Cascadia margin compared to such places as Japan, precludes using GPS vertical velocities as strong constraints on subduction zone locking [e.g., *Aoki and Scholz*, 2003]. For Cascadia, the most precise vertical velocity data remain the regional leveling conducted by the NGS and measurements of relative sea level at the continuously operated National Ocean Service (NOS) tide gauges. However, both historical data sources contain errors which must be corrected to avoid biased uplift rates. The leveling data contain errors due to systematic and random survey error as well as bench mark instability. Relative sea level trends at some tide gauges are biased by instabilities of bench marks that maintain the local vertical reference frames. Here we use the multiple observations of relative bench mark elevations along each leveling

line and local tidal loop to identify and remove such errors from the vertical geodetic data. Both the leveling and sea level uplift rates are made more robust by using additional historical data that have not been analyzed in previous regional compilations. We combine the spatially dense relative tilts given by releveling with the sparse estimates of absolute uplift rates at the tide gauges to obtain an internally consistent vertical velocity field with associated errors for western Oregon and northwesternmost California. Using an elastic dislocation model, we invert this vertical velocity field for the distribution of locking on the Cascadia subduction zone.

2. Relative Uplift Rates From Tidal Data

[7] We have extended and reanalyzed the tidal records for the six southern Cascadia outer coastal sites previously used by *Mitchell et al.* [1994]. These continuous tidal gauges, operated by the National Ocean Service (NOS), are distributed along the coast from Crescent City, California, to Astoria, Oregon (Figure 1). We use the verified monthly mean water level values provided over the Internet by the NOS, updated through December 2006. In addition to the 14 years that have elapsed since the *Mitchell et al.* [1994] analysis, we have extended the four shortest records by digitizing 67 months of hourly archived observations made in the 1920s, 1930s, and 1950s. To place these historical data into the same local vertical reference frame as the more recent continuous measurements at each site, we analyzed the results of repeated leveling of the tidal bench marks by the NOS and NGS. At each site we have identified the most stable bench marks, and we use the surveys between these bench marks and the different tidal staffs to tie the different epochs of observations into a common reference frame.

[8] For each tidal record we remove a mean seasonal cycle, identify and exclude data with clear errors, and correct for effects of bench mark instability (Appendix A). Instability of bench marks that were used to define tide gauge vertical datums bias parts of the Astoria and South Beach records at levels of 5.0–1.6 mm a^{-1}, and other tide gauges at lower levels before correction (Appendix A). Additionally, for the Astoria gauge in the mouth of the Columbia River, we remove an average effect of river discharge on measured water level (Appendix A). To determine the rate of relative sea level rise at each site we fit a least squares linear regression trend to the time series. The rates are relative in that they record the change in water level with respect to the local crust which is moving at some vertical velocity. We calculate uncertainties of the linear relative sea level rates using the Hildreth-Lu procedure [*Neter et al.*, 1990] to account for temporal autocorrelation in the time series (Appendix B and Table 1). Sea level time series with best fit linear trends for the six outer coast tide gauges are shown in Figure 2a.

[9] Much of the noise left in the seasonally corrected time series of Figure 2a is shared from site to site and represents

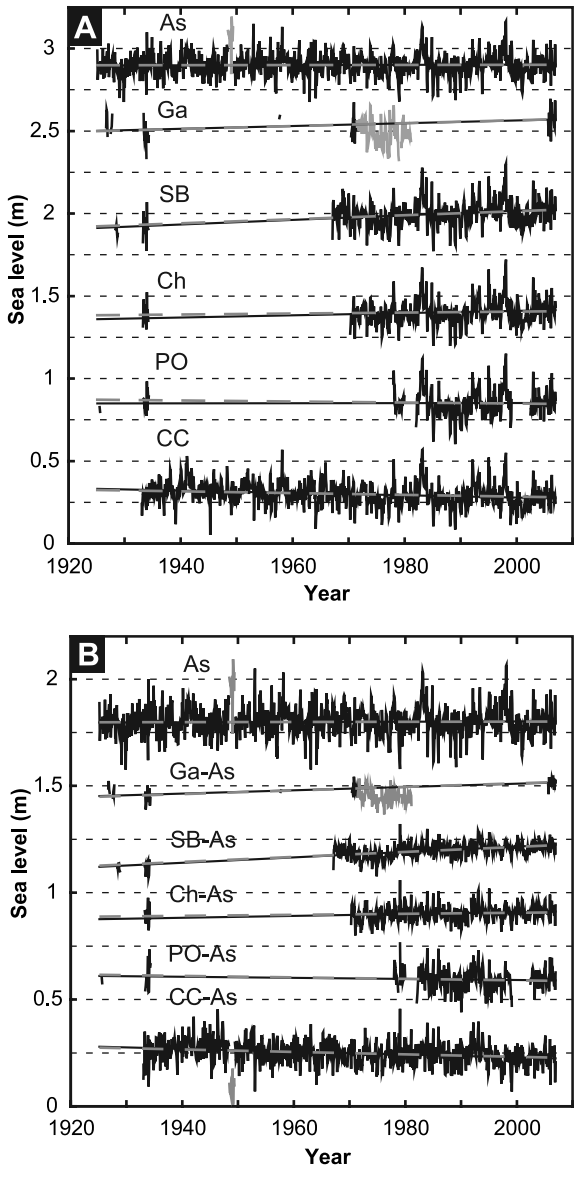

Figure 2. Sea level time series collected by National Ocean Service for Oregon portion of Cascadia. (a) Time series for each gauge, corrected for instabilities of primary bench marks, with site-specific mean seasonal cycle removed, and river effect removed for Astoria. See Figure A4 for example of processing. We have extended the records of the four central tide gauges with archived pre-1960 data to better constrain the relative sea level trends over the last century, and all records are updated through 2006. Gray data from Astoria and Garibaldi are excluded from the analysis (Appendix A). Straight black lines are linear regression fits, and the dashed gray lines have the slopes determined from the least squares adjustment, which incorporates the rates from the more precise differenced time series (see Table 1 for values). Note that the adjustment only modifies the trends slightly, but this increases the confidence in the values of the trends. (b) Example of differenced time series, using Astoria. Top As time series is same data shown in Figure 2a. Note the change in scale. Below are the differences of Astoria from each of the other sites, arrayed north to south. Note that the scatter around the regression lines is reduced compared to the original time series, as shared ocean noise is removed. The scatter around the trend lines increases as the sites become more widely separated (moving down in the figure).

Table 1. Observed and Adjusted Relative Sea Level (RSL) Rates

Site or Difference	Observed RSL Rate (mm a^{-1})	Autocorrelation Parameter (ρ)[a]	SE From Linear Regression (mm a^{-1})	SE From Hildreth-Lu[a] (σ_{ts}) (mm a^{-1})	Adjusted RSL Rate (mm a^{-1})	Residual (v) (mm a^{-1})	v/σ_{ts} (%)	Adjusted SE (σ_{tg}) (mm a^{-1})
CC	−0.71	0.48	0.11	0.18	−0.54	0.17	93	0.08
PO	0.04	0.52	0.32	0.62	−0.31	−0.35	−56	0.10
Ch	0.66	0.49	0.26	0.45	0.29	−0.38	−84	0.09
SB	1.39	0.46	0.23	0.38	1.22	−0.17	−45	0.08
Ga	0.85	0.05	0.31	0.38	0.88	0.04	9	0.09
As	0.06	0.32	0.09	0.13	0.04	−0.02	−18	0.07
CC-PO	−0.05	0.48	0.13	0.23	−0.23	−0.19	−82	
CC-Ch	−0.79	0.32	0.11	0.15	−0.82	−0.03	−22	
CC-SB	−1.58	0.27	0.12	0.17	−1.76	−0.17	−104	
CC-Ga	−1.27	0.11	0.29	0.34	−1.42	−0.16	−45	
CC-As	−0.67	0.27	0.08	0.11	−0.58	0.09	84	
PO-Ch	−0.53	0.45	0.12	0.20	−0.59	−0.07	−34	
PO-SB	−1.55	0.43	0.14	0.24	−1.52	0.03	11	
PO-Ga	−1.13	0.11	0.27	0.32	−1.19	−0.06	−18	
PO-As	−0.26	0.38	0.19	0.31	−0.35	−0.08	−27	
Ch-SB	−0.96	0.48	0.07	0.12	−0.93	0.03	21	
Ch-Ga	−0.79	0.15	0.20	0.25	−0.60	0.20	77	
Ch-As	0.44	0.32	0.12	0.18	0.25	−0.19	−108	
SB-Ga	0.30	0.10	0.12	0.14	0.33	0.03	21	
SB-As	1.26	0.41	0.09	0.13	1.18	−0.08	−58	
Ga-As	0.77	0.17	0.13	0.18	0.84	0.07	42	

[a]See Appendix B for details. RSL, relative sea level.

regional oceanographic noise. Differencing the record of one site from another removes the portion of the noise common to the two sites, along with the effect of the regional eustatic sea level rise. Thus, the trend of a differenced time series is the difference in sea level change between the two sites, or the crustal uplift rate of one site relative to the other. Nearby sites share the pattern of oceanographic noise quite closely and differenced sea level trends have much less uncertainty than those calculated from the seasonally corrected time series for one site (Figure 2b) [*Mitchell et al.*, 1994]. We differenced the time series of the 15 possible pairs of tide gauges in the six site set and calculated relative sea level rates and associated uncertainties (Appendix B and Table 1).

[10] The rate of relative sea level rise for each site may be determined from its individual time series or by using the rate determined at a different site and the relative rates of the two sites calculated from their differenced time series. Given the six sites considered here, there are six different estimates of the rate of sea level rise for each site, with associated uncertainties (Table 1). We have used a weighted least squares adjustment to incorporate the more precise constraints of the differenced rates into our estimate of the rate of relative sea level change for each site [*Wolf and Ghilani*, 1997]. Weights, w, are calculated as $w = \sigma_{ts}^{-2}$, where σ_{ts} is the standard error of the trend of time series as determined by the Hildreth-Lu approach.

[11] The relative sea level change rates from the individual sites and the intersite differences are quite consistent with one another along the Cascadia coast from Crescent City to Astoria (Table 1 and Figure 2). The adjusted values of the 21 relative sea level rates are all approximately one standard error or less from their initial observed values. The estimated standard errors of the adjusted rates of relative sea level change are all less than their initial values, ranging from 0.07 to 0.10 mm a^{-1}. The intersite comparisons are most effective in reducing the uncertainty of relative sea level trends for tide gauges with fewer months of observed data. The adjusted uncertainties of the sites with the shortest records are similar to the preadjustment standard errors of the long time series at Crescent City and Astoria (Table 1).

[12] The regional rate of absolute sea level rise in a geocentric reference frame allows the calculation of absolute crustal uplift rates from values of relative sea level rise. As the value of the regional rate of eustatic sea level rise is more difficult to determine and affects all of the sites equally, we first calculate relative uplift rates among the sites for initial comparison to rates obtained from leveling by using zero sea level change. The high precision of the rates of relative sea level rise at the tide gauges translates to a high precision of relative uplift rates between tide gauges. We later add the uncertain value of regional eustatic sea level rise to determine less precise absolute uplift rates (Section 4).

3. Relative Uplift Rates From Leveling Data

[13] We have calculated relative uplift rates using repeated first- and second-order leveling surveys along highways of western Oregon and northernmost California conducted by the National Geodetic Survey (NGS). We use the unadjusted line data, with orthometric, rod, level, temperature, astronomical, refraction, and magnetic corrections applied by the NGS as appropriate [*Federal Geodetic Control Committee*, 1984]. Most of the routes were first surveyed in the early 1930s and were then releveled both in 1941 and the late 1980s. The current data set has been previously analyzed and interpreted [*Mitchell et al.*, 1994; *Hyndman and Wang*, 1995; *Verdonck*, 2006]. Here we improve upon previous work by identifying and correcting errors in the data where possible, filling spatial gaps in the data by making secondary ties between nearby bench marks, better tying the leveling uplift rates to a sea level reference frame, and more rigorously calculating uncertainty of the uplift rates.

[14] The array of six permanent tide gauges breaks the coastal leveling route into five segments ranging in length from 115 to 174 km (Figure 1). We have analyzed the coastal

Table 2. Comparison of Tidal and Leveling Relative Uplift Rates

Coastal Segment	D (km)	Leveling Difference (mm a^{-1})	Tidal Difference (mm a^{-1})	Leveling Minus Tidal (mm a^{-1})
CC-PO	160	−0.04 ± 0.33	0.23 ± 0.19	−0.28 ± 0.38
PO-Ch	123	−0.08 ± 0.28	0.59 ± 0.26	−0.67 ± 0.38
Ch-SB	174	3.29 ± 0.36	0.93 ± 0.38	2.36 ± 0.52
Ch-SB[a]		1.62 ± 0.36		0.69 ± 0.52
SB-Ga	144	0.04 ± 0.36	−0.33 ± 0.44	0.38 ± 0.57
Ga-As	115	−0.28 ± 0.32	−0.84 ± 0.44	0.57 ± 0.54

[a]Ch-SB leveling relative uplift rate after correction of systematic error as discussed in Appendix C.

data in these five segments, as the uplift rates of bench marks in the vicinity of a tide gauge are well constrained by the tidal uplift rates, but bench mark uplift rates become more uncertain with increasing distance from the gauge due to progressive accumulation of random and systematic leveling error [*Vanicek et al.*, 1980]. Analysis of the raw leveling uplift rates in each segment suggest that the 1941 leveling was contaminated by systematic error, and we take the 1980s–1930s relative uplift rates as the best estimates (Appendix C). Differences in relative uplift rates across each segment determined by both leveling and tide gauges are equal within expected levels of error for all the segments except the central Charleston (Ch)–South Beach (SB) segment, where we infer and correct systematic error in the single-run 1980s leveling (Table 2 and Appendix C).

[15] The 1980s–1930s rates provide the best estimates of uplift rate due to the longer period over which deformation occurred and the higher quality surveying of the 1930s compared to 1941. However, the longest interval also means there are the fewest bench marks that were surveyed in both epochs due to route changes and bench mark destruction. We increase the 164 1980s–1930s "differences" by estimating the 1930s elevations of 179 bench marks that were monumented after the 1930s surveys or initially missed, using nearby monuments that were present in the 1930s but were not surveyed in the 1980s. Differential tectonic motion between points separated by $\leq$1 km is negligible, so measured elevation differences between such nearby points are essentially time-independent. This allows us to precisely determine bench mark elevations in the reference frame of the earliest leveling lines and yields more dense measurements which accurately estimate the regional-scale tilt signals when differenced from the 1980s leveling. While it may seem counterintuitive to find the elevation of a bench mark before it was constructed, this approach yields rates for bench marks that were present in the late 1980s and have potential for measurement in future surveys. We use three sources of additional information to calculate what we call "secondary" 1930s elevations: tidal surveying, reset elevations, and 1941 ties between nearby bench marks (Appendix D). We further densify uplift rate observations by estimating the 1941 leveling error and correcting the 1941–1931 differences (Appendix D). While these corrected 1941–1931 values are much less certain than those calculated from the longer intervals, they provide some information in gaps between the more precise measurements.

[16] We attach the relative uplift rates calculated from the leveling lines to the estimates of uplift rates at the six tide gauges with a weighted adjustment that takes into account uncertainty in both the leveling and tidal measurements (Appendix E). This provides a means to attach the leveling uplift rates to an absolute reference frame as well as to remove the effects of random and systematic leveling error that accumulate between tide gauges. This adjustment is made using relative tidal uplift rates, prior to inclusion of the rate of eustatic sea level rise, which is a relatively large source of uncertainty in the final absolute uplift rate that affects all of the bench marks equally. We attach the uplift rates for the three east-west leveling routes to stable-appearing bench marks on the adjusted coastal route and propagate errors east from the attachment point (Appendix E).

[17] We filter the set of uplift rates to remove bench marks with anomalous uplift rates due to local monument instability (Appendix F). We use local regression along run distance to define the most likely pattern of uplift rates along each route, and we only remove outlying points that are extremely unlikely to be the result of tectonic causes or surveying errors that would bias estimates of the regional uplift pattern. Most of the removed data are 1941–1930s rates that were not completely fixed by the interpolated correction. Of the 9% of the total long interval rates that we removed, 86% had lower uplift rates than their neighbors, showing that settling is more common for at least the most unstable bench marks. This may suggest that bench mark instability at undetectable lower levels may bias mean uplift rates to slightly lower values as well (Appendix F).

4. Absolute Uplift Rates From Sea Level Rise

[18] To infer absolute crustal uplift rates from the calculated rates of sea level change requires a value for the regional rate of geocentric sea level rise over the period of observations for Cascadia. Previous studies of Cascadia tide gauges have used global estimates of the rate of sea level rise that vary between 1.0 and 2.4 mm a^{-1}, with the more recent work using 1.8–2.0 mm a^{-1} [*Holdahl et al.*, 1989; *Savage et al.*, 1991; *Mitchell et al.*, 1994; *Hyndman and Wang*, 1995; *Verdonck*, 2006]. Studies of global sea level rise have sought to quantify spatially averaged change in sea surface height due to addition of water mass to the oceans as well as thermal expansion. This global sea level rise is the primary signal in individual tide gauge records, but superimposed upon it are variations caused by regional redistribution of ocean volume such as El Niño–Southern Oscillation (ENSO) [*Douglas*, 2001]. The effects of these regional perturbations are fairly large relative to the total water level change in the 20th century, and their recurrence is temporally nonuniform (Figure 2). Thus, the rate of sea level rise calculated from a single tide gauge record is sensitive to both the gauge's location and the time period of the record. A regional sea level record of the appropriate length, not contaminated by crustal motion, is required to accurately remove the component of the linear trend of a sea level time series contributed by both global sea level rise and regional oceanographic variation.

[19] Since the 1992 launch of the TOPEX/POSEIDON sensor, satellite altimetry has allowed a precise global view of sea level variation in a geocentric reference frame. The satellite time series is currently too short to determine robust estimates of the rate of sea level rise on a regional basis, due to temporally and spatially variable oceanographic effects such as ENSO. *Church et al.* [2004] used the satellite data coupled

with a worldwide network of tide gauges to reconstruct a global sea level history for the period 1950–2000, obtaining a spatially averaged value of 1.8 ± 0.3 mm a^{-1}. However, the reconstructed time series for grid points offshore of Cascadia have slopes of 2.2 ± 0.3 mm a^{-1}. Extending this analysis with lowered spatial resolution back to 1870, *Church and White* [2006] showed that global sea level rise accelerated around 1930. The longer reconstruction yields a globally averaged rate for the 20th century of 1.7 ± 0.3 mm a^{-1}, and a Cascadia rate of 2.0 ± 0.3 mm a^{-1}. The reconstructed sea level histories of these analyses generally match the temporal variations observed in Cascadia time series. However, as the reconstructions are globally constrained, the residual scatter around linear trends for individual grid points does not match in detail that observed at nearby tide gauges.

[20] The record of the Seattle, Washington tide gauge matches the geocentric reconstructions for Cascadia, and its distance from the trench suggests minimal interseismic deformation. The observed rates of relative sea level rise at Seattle over the entire record and its 20th century subset are both 2.1 ± 0.1 mm a^{-1} [*Zervas*, 2001; *Verdonck*, 2006]. This rate closely matches the value from the reconstructed time series over the same interval [*Church and White*, 2006]. Moreover, the linear trend of the 1950–2000 subset of the Seattle record is 2.2 mm a^{-1}, the same value as the more detailed reconstruction of *Church et al.* [2004]. On the basis of the agreement between the relative sea level rise rate at the Seattle tide gauge and the absolute sea level rise rates from the geocentric reconstructions, we conclude the uplift rate at Seattle is essentially 0 mm a^{-1}. A recent analysis of vertical GPS velocities and northern Cascadia tidal records suggested that the absolute rate of sea level rise is 1.7 ± 0.5 mm a^{-1}, and Seattle is subsiding at 0.6 ± 0.9 mm a^{-1} [*Mazzotti et al.*, 2007]. This interpretation conflicts with models of subduction zone locking and postglacial rebound which both predict zero or positive uplift rates for Seattle [*Clague and James*, 2002; *Wang*, 2007]. Differences in reference frames and processing techniques yield vertical velocities for the SEAT GPS site that differ by up to 3.4 mm a^{-1} in six independent analyses [*Mazzotti et al.*, 2007; *Snay et al.*, 2007]. Given the current level of uncertainty in vertical GPS velocities and the consistency between the Seattle tide gauge record and the global sea level reconstructions, we use the Seattle tidal time series to estimate the absolute sea level rate contribution to the relative water level trends observed at other Cascadia tide gauges.

[21] In using the between-site differences and the adjustment procedure to refine estimates of sea level change at the tide gauges, we essentially force the rate of linear eustatic sea level rise to be a single regional value. The magnitude of the adjusted regional rate of sea level rise is determined by the observed values and corresponding weights of sea level rates for the individual tide gauge time series. We make subsets of the Seattle record to match the months of data collected at each of the six southern Cascadia tide gauges. Linear trends fit to the Seattle subsets yield rates that range from 2.04 to 2.32 mm a^{-1}. Given the much greater amount of data collected at Astoria (As) and Crescent City (CC), the value calculated from the weighted adjustment is largely controlled by these two sites. The rates of the Seattle subsets for As and CC are 2.32 and 2.29 mm a^{-1}, respectively. The weighted mean of all six sites is 2.28 ± 0.03 mm a^{-1}. We add this value to all the adjusted uplift rates of bench marks to calculate absolute uplift rates. To account for possible deviations in eustatic sea level rate from the behavior at Seattle, we add in quadrature an additional 0.2 mm a^{-1} to the adjusted uncertainties.

5. Spatial Pattern of Vertical Velocity

[22] Absolute uplift rates for releveled bench marks in western Oregon and northernmost California are presented in Figure 3 (auxiliary material Data Set S1).[1] Similar to previous analyses of the tidal and leveling data [*Mitchell et al.*, 1994; *Verdonck*, 2006], we find two loci of higher uplift rate in southern and northern Oregon separated by a region of minimal uplift at the latitude range of ~44–45°N. Along latitudinal transects, uplift rates systematically vary from high values near the coast to lower values inland. The average magnitude of our uplift rates is higher than previous estimates due to the recognition of the post-1930 rate of eustatic sea level rise at Cascadia being higher than the global 20th century average. Additionally, the corrected errors in the South Beach and Astoria tidal records, the exclusion of the biased 1941 leveling data, and the correction of the 1988 leveling error between Charleston and South Beach all make the tidal and leveling data sets more consistent with one another. As a result of the greater rate of sea level rise and corrected South Beach tidal record, we infer that no portion of the Oregon Coast Range is currently undergoing regional-scale subsidence, as suggested previously [*Mitchell et al.*, 1994; *Verdonck*, 2006]. This is more consistent with models of subduction zone locking constrained with horizontal GPS velocities, which predict positive uplift rates well into the Coast Range, and even the Willamette Valley (Figure 1) [*Wang et al.*, 2003; *McCaffrey et al.*, 2007]. Regional contemporary subsidence of the central Coast Range is also at odds with geologic observations of uplifted marine terraces along the coast and stream incision within the range [*Personius*, 1995; *Kelsey et al.*, 1996].

[23] Projecting the uplift rate data perpendicular to the local strike of the subduction interface gives insight into the source of the uplift rate pattern (Figure 4). The data from the central Oregon coast (north of South Beach to north of Port Orford) all lie scattered around a single concave-up curvilinear trend similar in form to that predicted by an elastic dislocation model of a locked fault slipping at depth [*Savage*, 1983]. Most of the short-wavelength variation in uplift rate along the north-south coastal leveling route correlates with the distance of each bench mark from the trench. This geometric effect does not explain the high uplift rates in coastal northern Oregon, which is located above the same depth on the slab as the South Beach area. The profile along the Columbia River (As-east) has a concave-up eastward decline in uplift rate which is quite similar to the profile from the Coos Bay area, although shifted downdip. The northward transition to higher uplift rates occurs over a ~120 km along-strike interval from north of South Beach to north of Garibaldi (44.8°N to 45.85°N; Figure 3). Northward through this area, the coastal leveling route generally traverses downdip, so one would expect a decrease in uplift, but uplift rates have a net increase of approximately 1 mm a^{-1}. Superimposed on the northward

[1] Auxiliary materials are available at ftp://ftp.agu.org/apend/jb/2008JB005679.

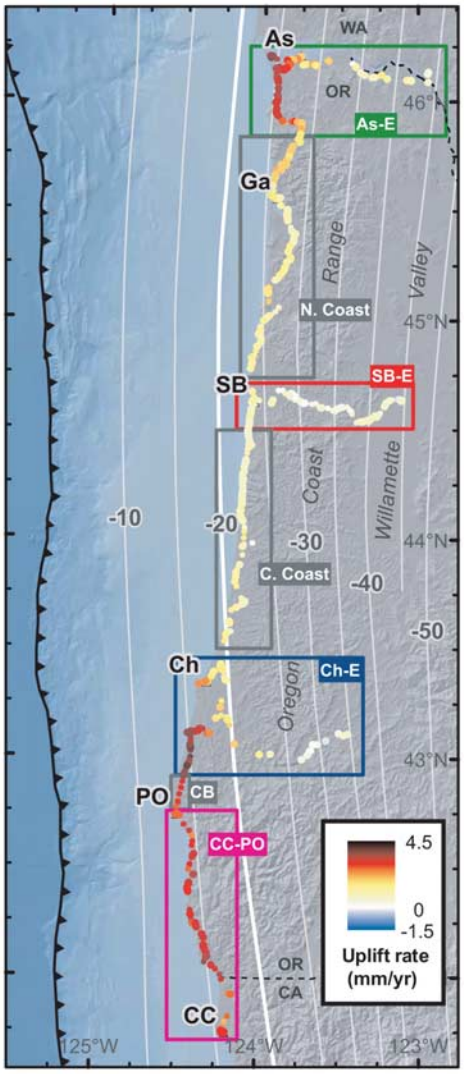

Figure 3. Uplift rates for bench marks along releveled routes in western Oregon and northernmost California are colored by the scale in the lower right. Labels indicate tide gauges used to name areas: As, Astoria; Ga, Garibaldi; SB, South Beach; Ch, Charleston; PO, Port Orford; and CC, Crescent City. In the central part of the map, uplift rates vary systematically, with the greatest values occurring above updip portions of the slab and declining inland. The southernmost section (CC-PO) has lower uplift rates despite being slightly updip relative to the central area. Note the contour-parallel gradient in uplift rates from SB-north to As. The line east from As shows a similar downdip decrease in uplift rate, although shifted downdip relative to the slab compared to the central area. The highlighted −20 km contour is used to project the data to a common trend line in Figure 4, accounting for the broad wavelength variation in the geometry of the subduction interface. The colored boxes correspond to the groupings of data in Figure 4.

increasing uplift rate trend, shorter-wavelength (tens of kilometers) variations in uplift rate generally correlate with east-west segments in the overall north-south leveling route, with bench marks to the west having higher uplift rates. The peak in uplift rate occurs north of Port Orford, near 43.0°N, with bench marks south and updip uplifting at lower rates than those to the northeast. The southernmost area near Crescent City, California, lies at a downdip distance that is equivalent to the peak in uplift observed near Bandon, Oregon; however, the southernmost uplift rates are ∼1 mm a^{-1} lower. This requires an along-strike change in the uplift rate pattern somewhere near Port Orford.

[24] Uplift rates from both the Charleston and South Beach areas decline along the leveling lines east from the coast, reaching minima of 0.2–0.3 mm a^{-1} near the −30 km slab contour (Figure 3), which is ∼40 km east of the −20 km contour that we use as our spatial reference (Figure 4). Inland from these points, uplift rates increase ∼0.5 mm a^{-1}, reaching a maximum near the −40 km contour and the western margin of the Willamette Valley along the SB-east profile, which extends farthest east (Figure 4). The northernmost line, east from Astoria, shows a similar pattern of eastward reversal in the sign of the uplift rate slope, with the minimum being shifted eastward compared to the areas south, and the maximum again occurring near the −40 km slab contour (Figure 3). While these variations are within the expected error given the distances and lack of absolute uplift rate control on the east ends of the lines, the similarity between the three independent lines suggests that the data record regional uplift of the eastern Oregon Coast Range (Figure 4).

6. Cascadia Subduction Zone Locking

6.1. Modeling Methodology

[25] We model the pattern of interseismic deformation using a numerical model of the Cascadia subduction zone. The three-dimensional subduction interface geometry of *McCrory et al.* [2004] is discretized into planar triangular subfaults. Static Green's functions calculated by the boundary element program Poly3D are used to model surface displacement rates assuming an elastic half-space [*Thomas*, 1993]. We use a back slip methodology [*Savage*, 1983] where the convergence rate is calculated at each subfault on the plate interface using the Euler pole for Juan de Fuca–Oregon Coast Range convergence from *Wells and Simpson* [2001]. The slip rate deficit on each subfault is assigned the full convergence rate in the locked zone. In the transition zone, the slip rate deficit decreases with depth using the exponential decay function of *Wang et al.* [2003]. This limits the number of free parameters to two variables along any downdip profile, namely, the lower depth of the locked zone and the lower depth of the transition zone. Many subduction zones exhibit an aseismic portion of the plate interface updip of the locked zone nearest the trench. Our observations are largely insensitive to strain accumulation from this updip section because it is far from the onshore bench marks. We therefore assume that the subduction zone is locked all the way up to the trench in our models. As discussed by *Wang* [2007], this kinematic treatment is appropriate given that the locked zone likely prevents a possibly uncoupled section nearest the trench from moving during the interseismic period.

[26] The observed uplift rate data provide the strongest constraints on subduction zone locking where the leveling routes traverse inland from the coast, giving a downdip-oriented uplift rate profile. In light of this, we initially fit data from the four geographic sets that extend to the east:

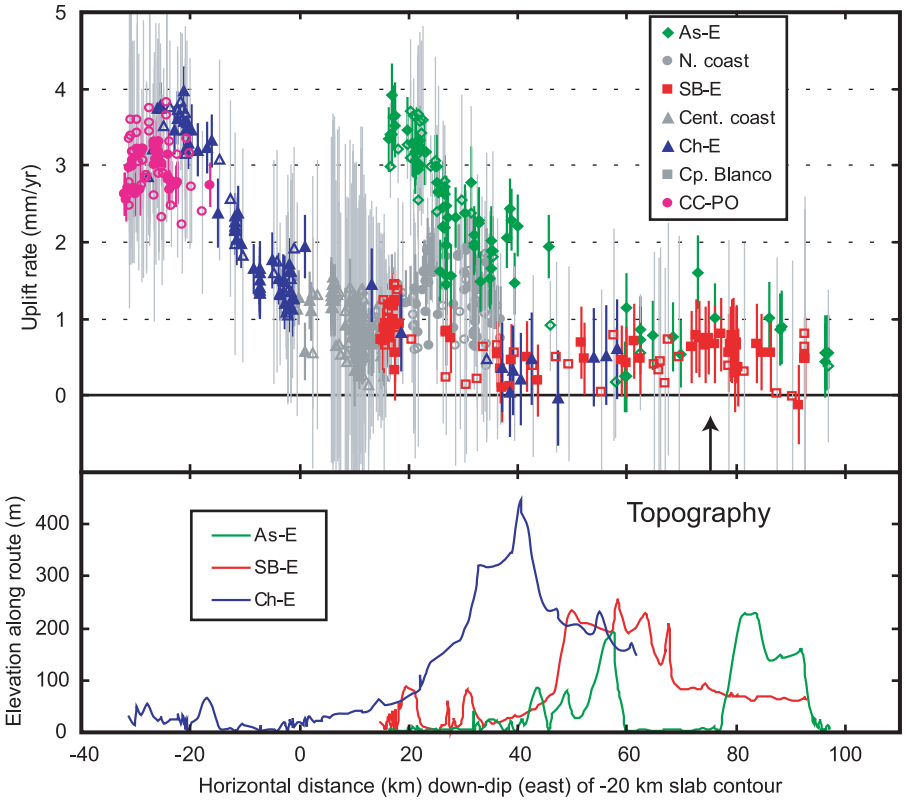

Figure 4. (top) All uplift rates for the coastal Oregon study area, projected to a line locally perpendicular to the −20 km slab contour. Points are color-coded by geographic boxes. See Figure 3 for locations of data and boxes. Filled symbols with colored error bars are long interval differences (>30 years), and open symbols with light gray error bars are less precise rates from shorter intervals. Data from the central Oregon coast (Ch-E plus Central Coast plus SB-E) cluster around a common concave-up trend, where most of the variation in uplift rate can be explained by position relative to the subducting slab. The southernmost data (CC-PO) follow a slightly different trend. The greatest deviation from the central area occurs in the northernmost box (As-E), where a similar concave-up trend is offset to greater uplift rates given its distance from the trench. Note that rates from the eastern ends of the eastern leveling lines do not scatter around zero uplift rate but instead rise from minima near 40 km to maxima near 75 km (shown by arrow), which roughly corresponds to the −40 km slab contour, and the eastern edge of the central Oregon Coast Range. Although these inland uplift rates are not significantly different from zero at a high level of confidence, the similar pattern on three independent leveling routes gives greater weight to this observation. (bottom) Note that the position of steep topography traversed by the three eastward lines occurs in different places along the leveling routes, suggesting that topography-related leveling errors are not responsible for the along-strike consistency of inland uplift rates.

As-east, SB-east, Ch-east, and CC-Port Orford (PO) (see Figure 3 for locations). For each geographic set, we systematically explore the sensitivity of the data to the depths of the transition and locked zones through a grid search of the parameter space (Figure 5). Interseismic uplift rates are predicted at the locations of the releveled bench marks, and the goodness of fit of the possible model configurations are determined by comparing predicted to observed uplift rates with a weighted RMS error per degree of freedom. The data are weighted assuming a diagonal covariance matrix. The fits for the SB-east and Ch-east groups require nearly identical model parameters, confirming the observation that all of the data between 43.0°N and 44.8°N cluster around a common trend in the profile of Figure 4. Consequently, we lump the data of the SB-east, Central Coast, and Ch-east groupings into a common geographic set, and find the best fit locking parameters for this entire group. With the combined central data set, most of the data from western Oregon can be divided into three distinct subgroups, each requiring a unique set of locking parameters (Figure 5).

[27] To infer how the pattern of locking transitions from one of the three well-constrained areas to the next, we use a spline to interpolate the along-strike locking pattern. Over these intervening reaches, the basal depths of the locked and transition zones change monotonically from the southern to northern sets of locking parameters. We fit the spline by systematically adjusting its curvature and flexure point. We optimize the interpolated locking pattern with a systematic investigation of possible spline shapes, using the misfit to the observed bench mark uplift rates from the intervening north-south section of the coastal leveling route as the

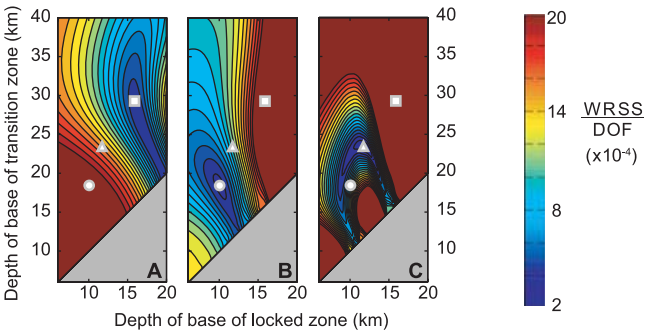

Figure 5. Model misfit plotted as a function of the downdip extents of the locked and transition zones for three data subsets: (a) As-east leveling route, (b) central coast and eastward leveling routes, and (c) CC-PO. See Figure 3 for locations of the subsets. Gray shaded region is outside the permissible model space. The minima for the different areas are plotted in each frame as three white shapes: As-east, square; central, circle; and CC-PO, triangle. Although there is some acceptable trade-off between the locked and transition zone depths for each area, the data require distinct sets of locking parameters within these geographic boxes.

criterion to determine goodness of fit. The spacing of the east-west leveling routes makes the leveling data best suited for imaging variations in locking on the scale of 100–200 km along strike. However, the tight clustering of uplift rate data around common trends for each of the geographic sets when projected in Figure 4 shows that finer-scale variations within these geographic boxes are not dramatic.

6.2. Locking Pattern for Oregon Portion of Cascadia

[28] Applying the modeling procedure described above to the western Oregon uplift rate data yields a best fit locking pattern shown in Figure 6. All three of the geographic areas (As-east, SB-east plus Central Coast plus Ch-east, and CC-PO) have distinct sets of locking parameters with nonoverlapping minima in misfit (Figure 5). The Astoria area requires the most deeply locked interface, consistent with the uplift rates being highest in the northern area, for a given depth to the slab (Figure 4). The central area has a well-constrained minimum in misfit; however, the fit for these data is largely controlled by the data from the Ch-east area, as the position of the steep uplift rate gradient is the most diagnostic feature. Although the data from the SB-east area are well fit by the locking parameters for the combined central area, these data could be equally well matched with less or even no locking at this latitude (44.6°N).

[29] The southern (CC-PO) area requires a different set of locking parameters from the areas to the north. As we model this area, the base of the locked zone is similar to the central area, but the transition zone extends deeper than the areas to the north (Figure 6). Partial locking in the transition zone extends downdip below the coastline along the CC-PO section, and is the only area where we infer significant slip rate deficit accumulating below land. However, the locking for this area is not as well resolved as for the areas to the north with east-west leveling routes, as the only releveled route through the southern geographic box trends obliquely to the strike of the subduction interface. We model the observed variation in uplift rates between PO and CC as a result of the leveling route traversing downdip across an area of consistent locking. We cannot rule out the possibility that the locking parameters vary along-strike within the CC-PO section of the margin. If this is the case, the abrupt along-strike decrease in uplift rate north of PO may instead represent the locked zone progressively narrowing offshore relative to the areas to the north. We prefer minimal along-strike variation as the simplest explanation for the data. Additional vertical geodetic data gathered by reoccupying historic leveling bench marks and tide gauges in additional coast-perpendicular transects offer the potential to better resolve this issue [*Burgette et al.*, 2005].

[30] As we model the data with three geographic areas with coherent uplift rate patterns, there are two intervening along-strike changes in locking parameters. For the southern transition between the Port Orford tide gauge and the southernmost bench marks of the Ch-east box, the short distance requires an abrupt along-strike change in the depth of the base of the transition zone (Figure 6). The model produces a much more gradual along-strike change between the SB and As areas, where the locking depth increases to the north, but the width of the transition zone maintains an approximately constant width.

[31] In general, the preferred model describes the observed uplift rate pattern well (Figures 7 and 8). The standard deviation of the residuals is 0.35 mm a^{-1}, similar to the mean standard error of the long interval uplift rates, 0.40 mm a^{-1}. Areas of spatially correlated residuals of one sign could be better fit by making the locking pattern vary along strike on a smaller spatial scale. This is most apparent along the coastal route between South Beach and Astoria (Figure 7). The Garibaldi area is consistently negative, and it is flanked north and south by areas of positive residuals. This systematic mismatch is a consequence of the monotonic change in locking depths required by our interpolation scheme between the South Beach and Astoria east-west profiles. A similar situation exists in the Coos Bay area, near the Charleston tide gauge (Figures 7 and 8). Allowing the locking depth to vary more along-strike would improve the fit in these areas, but it would also increase the number of free parameters. Given the general agreement of the model and data within error, we choose not to increase the complexity of the model.

[32] Spatially correlated residuals also occur in the Oregon Coast Range (OCR) where the lines traverse east. There are positive residuals on all three lines near their eastern ends, with maxima near the −40 km contour near the eastern margin of the OCR (Figure 7). In contrast with the coastal areas of systematic misfit, modifying the model locking pattern will not improve the under fit to these eastern data without producing an even worse fit near the coast. We experimented with models that produce zero uplift on the eastern ends of the leveling profiles by subtracting a constant from the entire data set. However, the gross features of our locking model were unchanged, suggesting that the locking model is insensitive to uplift along the eastern OCR. The eastern high residuals likely reflect tectonic uplift of the Coast Range, as dissimilar topographies of the three eastern leveling routes are unlikely to have produced the similar uplift rate patterns through surveying error (Figure 4). The peak in uplift rate in the eastern OCR matches geologic suggestions of relative uplift along the eastern margin of the Coast Range [*Baldwin and*

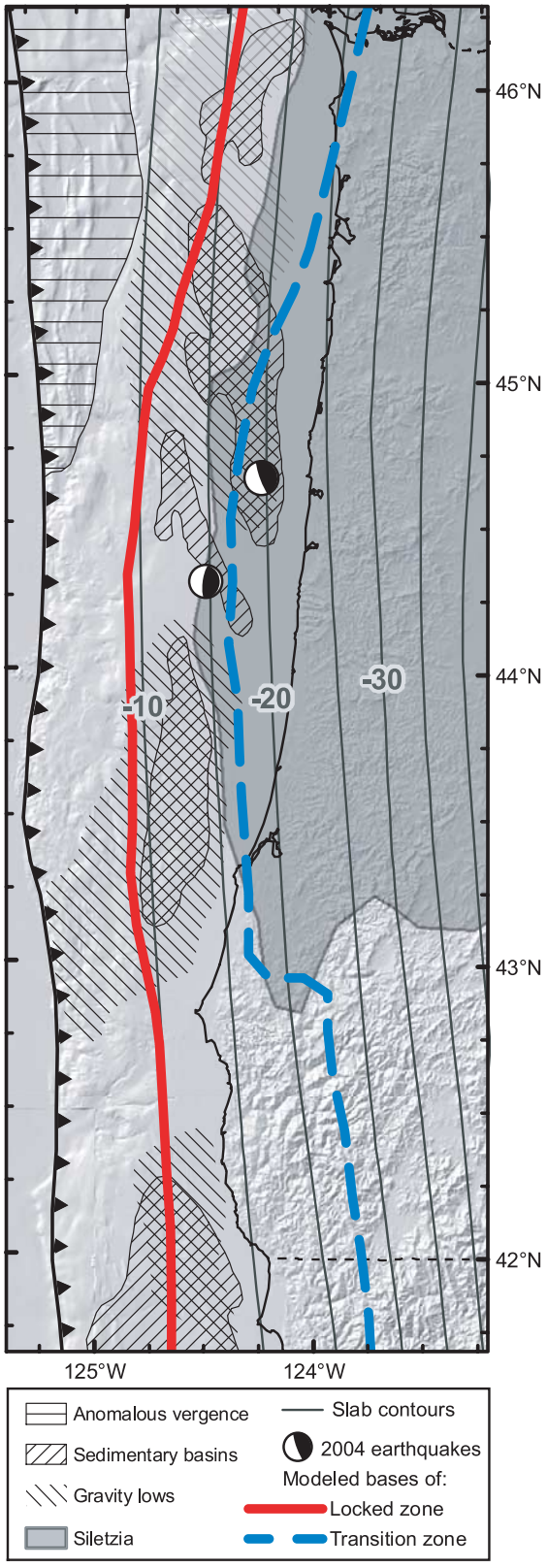

Howell, 1949; *Moeller*, 1990; *Almond et al.*, 2007]. However, the highest positive residual uplift rates continue into the Willamette Valley, at odds with the geologic observations of differential uplift along the eastern edge of the OCR. Another possibility is that the rigid Siletzia block, which underlies most of the fore arc, is interseismically tilting down to the west as it is being elastically strained. In this model, interseismic uplift of the eastern OCR and Willamette Valley would be reversed in a coseismic event. The positive interseismic uplift rates we find throughout the OCR are compatible with a small fraction of the interseismic strain being unrecovered during coseismic release and contributing to the inferred long-term uplift of the Coast Range [*Kelsey et al.*, 1994]. However, the east-west gradient in interseismic uplift we observe does not appear to be reflected in the Coast Range topography, making a direct link between elastic strain accumulation and long-term rock uplift in the OCR speculative. Alternatively, long-term uplift of the OCR may be the result of other dynamic subduction processes.

[33] The inferred locking pattern from this study is broadly consistent with previous efforts to model locking on the Cascadia subduction zone, although there are important differences (Figure 9). South of 45°N, the width of the best fit locked zone from our model is similar to that of *Flück et al.* [1997], which was based on vertical geodesy and thermal modeling [*Hyndman and Wang*, 1995], although the magnitude of slip rate deficit is lower for our model. To match the higher uplift rates north of 45°N, we require a deeper locked zone than inferred by prior studies depicted in Figure 9. More recent models constrained by horizontal GPS velocities are best fit by wider transition zones than our model (Figure 9) [*Wang et al.*, 2003; *McCaffrey et al.*, 2007]. This contrast is most prominent for the *McCaffrey et al.* [2007] model in central and southern Oregon, which predicts interseismic subsidence of the coastal area around the Charleston tide gauge, where we observe uplift rates of ~2 mm a^{-1}. The nonlinear taper of slip in the transition zone implemented in our model has a relatively subtle effect on the predicted extents of the locked and transition zones compared to the linear decay of the *Flück et al.* [1997] model, so this parameter alone does not explain the difference (Figure 9). The

Figure 6. Modeled extents of the locked and transition zones, compared to major geologic features of the Cascadia fore arc. The subsurface extent of the mafic Siletzia block is generalized from local and regional studies of the fore arc [*Wells et al.*, 1998; *Parsons et al.*, 1999; *McNeill et al.*, 2000; *Blakely et al.*, 2005]. Note that the modeled locked and transition zones vary along strike, following the trend of the western edge of Siletzia offshore of central and northern Oregon. The abrupt along-strike change in locking in southern Oregon corresponds to the southern end of Siletzia. Major offshore fore-arc gravity lows and associated basins [*Wells et al.*, 2003] generally lie near the western edge of Siletzia and overlie the lower part of our locked zone and much of the transition zone. The northern change in locking is also paralleled by a northward widening area of landward to mixed vergence in the outer accretionary wedge [*Mackay et al.*, 1992; *Gutscher et al.*, 2001]. Focal mechanisms show locations of 2004 earthquakes inferred on the plate boundary [*Tréhu et al.*, 2008].

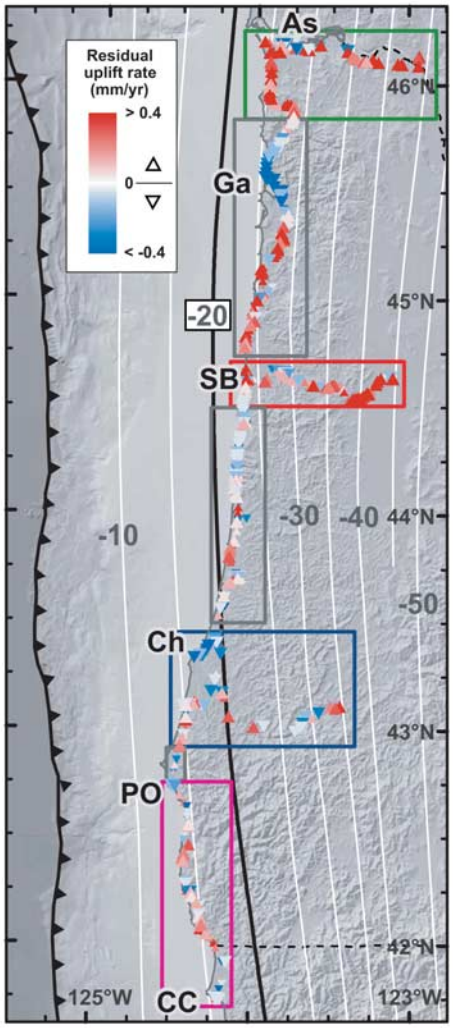

Figure 7. Spatial pattern of model misfit to data from the best fit locking pattern (Figure 6), calculated as observed minus predicted. The color scale is stretched over approximately one standard deviation to emphasize the sign of deviations. Positive residuals are north pointing triangles; negative residuals are shown by south pointing triangles.

general discrepancy between the narrow transition zone that better predicts vertical data and the wide transition zone that better fits the horizontal GPS velocities is a persistent feature of Cascadia elastic dislocation models. One notable difference between the data sets is the 50–80 year time period over which the leveling and tidal uplift rates are averaged, compared to the 10–15 year of GPS measurements. Also, the modeling of the horizontal GPS data requires a correction for the rotation of western Oregon.

[34] Other models that explored locking with more simple geometries also give results that follow the general trend of ours. Models of horizontal data without a transition zone produce locked areas that are slightly larger than our locked zone and show deeper locking in northern Oregon than southern, although the along-strike pattern is not finely resolved [*Savage et al.*, 2000; *Svarc et al.*, 2002]. Horizontal strain data are also consistent with a northward deepening of locking from central to northern Oregon [*Murray and Lisowski*, 2000].

[35] Viscoelastic modeling of the Cascadia subduction zone, with locked and transition zones similar to the *Flück et al.* [1997] model, predicts modern convergence-parallel horizontal velocities well into the fore-arc valleys [*Wang*, 2007]. Predicted uplift rates from this viscoelastic model reach zero in the Oregon Coast Range. This more rapid eastward decay in uplift rate is more consistent with the vertical data presented here, although the essentially contour-parallel locking pattern of the *Wang* [2007] model does not reproduce the along-strike variations in uplift rate that we observe. The wide "effective transition zone" implemented in the elastic dislocation model of *Wang et al.* [2003] accounts for surface deformation due to viscoelastic mantle relaxation in addition to the strain from elastic interseismic coupling. As there are potential model tradeoffs in the extents of the locked and transition zones, using an elastic model with a wide effective transition zone to capture the viscoelastic mantle response may bias the inferred extent of interseismic locking. The lower sensitivity of the vertical data to geologic processes such as viscoelastic relaxation and secular rotation of the fore arc make them a robust tool for determining the pattern of locking at Cascadia.

6.3. Regional Context of Cascadia Locking Variation

[36] The general correspondence of our modeled locked and transition zones to the limits inferred from thermal modeling supports the idea that temperature provides a first-order control on the downdip pattern of locking at the Cascadia margin [*Hyndman and Wang*, 1995]. However, the along-strike variations in locking suggest that isotherms on the interface are not parallel to slab depth contours or that other geologic controls play a role (Figure 6). Variations in locking correlate most strongly with the extent of the Siletzia block [*Wells et al.*, 1998]. The subsurface extent of the mafic Siletzia crust is known on a regional basis from seismic profiling, drill logs, and magnetic and gravity surveys [*Wells et al.*, 1998; *Parsons et al.*, 1999; *McNeill et al.*, 2000; *Blakely et al.*, 2005]. Along the portion of the Oregon margin where Siletzia underlies the offshore fore arc, there is a striking correlation between the western edge of the Siletzia block and the middle to lower transition zone of our model (Figure 6). Furthermore, the abrupt along-strike change in locking near Port Orford occurs at the southern boundary of Siletzia. South of this boundary, the accreted Klamath terranes form the fore-arc basement. The gravity high of the southern boundary of Siletzia is also associated with two of the more active transverse coastal structures [*Kelsey et al.*, 1996].

[37] Along the Oregon margin, the western extent of the Siletzia block also corresponds with the eastern edge of offshore fore-arc basins and associated gravity lows. Recent global studies have shown a spatial correlation between basin-centered fore-arc gravity lows and coseismic moment release in megathrust earthquakes [*Song and Simons*, 2003; *Wells et al.*, 2003]. Offshore of Oregon, fore-arc basins and associated gravity lows inferred by *Wells et al.* [2003] gen-

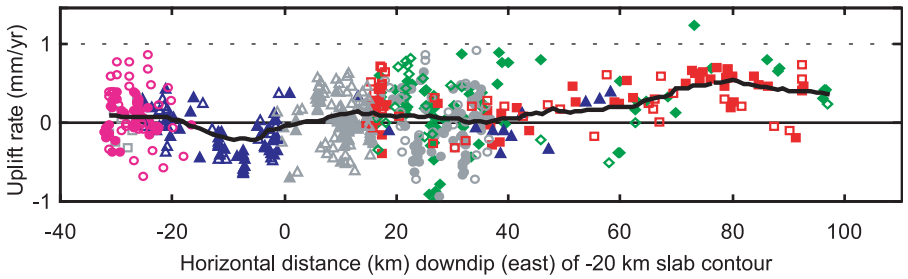

Figure 8. Model residuals (observed minus predicted) for all bench marks from the best fit model. Data are projected and colored by geographic bins in same manner as Figure 4. For map view distribution of residual uplift rates see Figure 7. Comparison to Figure 4 shows that the model explains the majority of the uplift rate variation observed in western Oregon. The black line is a mean calculated over a 20 km moving window. Some areas of systematic mismatch, such as the trough in the Ch-E data, could be improved by allowing the model locking to vary on a finer spatial scale. Note that the mean residual uplift rates are positive for the easternmost bench marks in the eastern Coast Range for all three profiles.

erally correspond to the lower portion of the locked zone and much of the transition zone in our model (Figure 6). The basin offshore of Astoria is shifted eastward relative to the slab depth contours, like the modeled locking depth and western limit of Siletzia. The causality responsible for the spatial association of gravity lows and seismic slip is a matter of debate [*Song and Simons*, 2003; *Wells et al.*, 2003; *Fuller et al.*, 2006], but the along-strike changes in the thickness and coherence of Siletzia may play a role in localizing the basins along the Cascadia margin.

[38] The correlation of the outer edge of Siletzia with the limit of partial locking along the subduction zone implies that the upper plate exerts a control on the limits of frictional interplate coupling. One possible control is the change in frictional properties associated with the downdip transition from sediments of the accretionary wedge to Siletzia. However, the mafic rock of Siletzia is unlikely to be in direct contact with the Juan de Fuca (JdF) oceanic crust along the plate interface over a large area where slip deficit is accumulating, if at all. Models of the fore-arc offshore of central Oregon based on seismic and potential fields data suggest that the locked zone as imaged here and in previous studies [e.g., *Flück et al.*, 1997], occurs where the downgoing slab is in contact with accretionary complex material [*Tréhu et al.*, 1994; *Fleming and Tréhu*, 1999; *Gerdom et al.*, 2000; *Blakely et al.*, 2005]. Inferred contact between Siletzia and the JdF slab is no higher than the lower part of the transition zone of our locking model [*Fleming and Tréhu*, 1999; *Gerdom et al.*, 2000; *Blakely et al.*, 2005]. Furthermore, observations of subducting sediment along this section of Cascadia [*Mackay et al.*, 1992; *Westbrook*, 1994; *Gulick et al.*, 1998; *Fisher et al.*, 1999; *Adam et al.*, 2004] suggest that the fault interface may occur within subducted sediment rather than between two intact bodies of mafic rock. Therefore, we conclude that the locking pattern is unlikely controlled by where Siletzia may be in direct contact with the downgoing plate.

[39] The heterogeneous thermal properties of the fore arc and advective heat transport from fluids may play an important role in controlling the along-strike variation in locking depths. The Siletzia block has lower thermal conductivity than the surrounding crust [*Hyndman and Wang*, 1995; *Oleskevich et al.*, 1999], and would insulate the Cascadia megathrust, resulting in slightly higher temperatures at the plate interface below Siletzia. Warmer temperatures on the plate interface would shift the locking depths updip. Thermal modeling predicts higher temperature on the plate interface due to the large extent of Siletzia in central Oregon, although the predicted value of the temperature increase is relatively small [*Hyndman and Wang*, 1995; *Oleskevich et al.*, 1999]. If the magnitude of this effect is greater than previously inferred, it would provide a systematic explanation for why the locking depths follow the western edge of Siletzia.

[40] The deeper locking in northern Oregon could also be the result of locally lower temperatures beneath the accretionary wedge caused by fluid expulsion from rapid wedge growth and compaction at the outlet of the Columbia River [*Westbrook*, 1994; *McNeill et al.*, 2000]. Rapid Pleistocene deposition may result in cooler temperatures on the plate interface than one would infer from the more common situation of steady sediment accumulation on the incoming oceanic plate. Heat advected through expelled fluids would offset the added insulation from increased sedimentation [*Hyndman et al.*, 1993] and force the locking depth downdip. However, such temperature effects are time-dependent and would depend on the details of when and how much sedimentation rates increased [e.g., *Hyndman et al.*, 1993]. If the locking is deeper in northern Oregon as a result of an along-strike change in temperature or sediment composition associated with the Columbia River, the geometry of Siletzia may play an indirect role in controlling this sediment delivery. The Columbia River follows a syncline that is likely localized by the change of thickness of the Siletzia block in northern Oregon [*Tréhu et al.*, 1994; *Parsons et al.*, 1999].

[41] The northern along-strike change in locking is also coincident with a change in the morphology and structural style of the outer accretionary wedge that also runs subparallel to the boundary of Siletzia. South of this change in locking (~44.8°N), the outer wedge has a steep bathymetric slope and imbricate thrusts have a consistent seaward vergence (Figure 6). North of this transition, the outer wedge has a lower slope, and the structures deforming the recently accreted sediments have landward or no preferred sense of vergence [*Mackay*

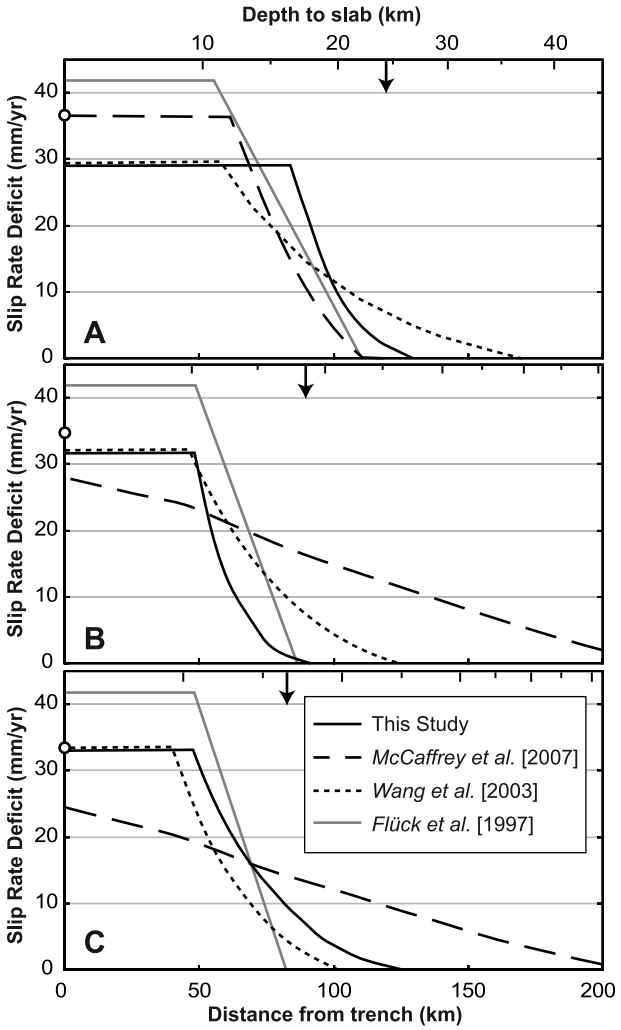

Figure 9. Comparison of published locking models for Oregon portion of Cascadia. Only distributed slip models on a 3-D plate interface are considered in this comparison. Plots show the downdip profiles of slip rate deficit along strike-perpendicular lines at (a) 46.0°N, (b) 43.5°N, and (c) 42.0°N plotted as a function of distance from the trench. Tick marks on the upper axis of each graph show the positions of slab contours at 5 km intervals [*McCrory et al.*, 2004]. As the slab dips more steeply to the south, the profile distance and relative spacing of these tick marks change between plots. The arrows show the position of the coast along each profile. All models use different parameterizations, such as the model geometry, the convergence rate, and the functional form of the downdip slip deficit profile, when solving for the locking distribution. The white dots show the full convergence rate at the trench for each profile from the *McCaffrey et al.* [2007] model, which is parameterized to allow partial slip over the entire depth range of the fault. Models constrained with uplift rate data [*Flück et al.*, 1997; this paper] generally have narrower transition zones than those constrained primarily by horizontal deformation data [*Wang et al.*, 2003; *McCaffrey et al.*, 2007].

et al., 1992; *Fisher et al.*, 1999; *McNeill et al.*, 2000]. These observations have been used to suggest that this portion of the outer wedge is exceptionally weak due to high pore pressures or anomalous sediment compositions relative to other parts of Cascadia [*Mackay et al.*, 1992; *Gutscher et al.*, 2001; *Underwood*, 2002; *Adam et al.*, 2004]. Along other subduction zones, marked contrasts in the behavior of the outer versus inner wedge have been correlated with the updip edge of the seismogenic zone [*Wang and Hu*, 2006]. If the updip limit of coseismic slip of the northern Oregon wedge is deeper than the areas to the south, it may mean that the locked zone maintains a nearly constant width along strike, as the change in wedge morphology nearly parallels the change in locking depth (Figure 6). Although kinematically this weak updip portion will still behave as part of the locked zone during the interseismic period, as discussed previously, it may not be appropriate to include the entire modeled locked zone in estimates of moment accumulation rates [*Wang*, 2007].

6.4. Interseismic Locking, Episodic Tremor and Slip, Seismicity, and Coseismic Subsidence

[42] The correlation between the extent of Siletzia and interseismic locking also appears to be reflected in the spatial pattern of episodic tremor and slip (ETS) along Cascadia. Both the northern and southern along-strike changes in locking correlate with observed transitions in recurrence frequency of ETS [*Brudzinski and Allen*, 2007]. Slip inversions for several northern Cascadia ETS events [*Dragert et al.*, 2001; *Szeliga et al.*, 2008] show the majority of slip occurs below the base of the transition zone as determined from vertical data [*Flück et al.*, 1997]. Although there have been limited observations of ETS deformation in Oregon, analysis of one event in central Oregon suggests slip occurred farther updip than most of the events imaged near the Columbia River to the north [*Szeliga et al.*, 2008]. Although future data will better resolve ETS in central Oregon, our locking model predicts a shallower ETS zone along this section of the subduction zone, assuming the ETS zone follows the base of the transition zone.

[43] The Cascadia plate interface has been largely aseismic over the instrumented period, especially in Oregon. However, a recent pair of earthquakes (M_w = 4.8 and 4.9) in 2004 have been identified and located by *Tréhu et al.* [2008]. These thrust events occurred offshore of central Oregon along the plate interface near the base of the transition zone as modeled here (Figure 6).

[44] The nature of strain release in the transition zone remains enigmatic. The narrower transition zone of our modeling and previous vertical studies suggests that most of the slip associated with ETS occurs downdip of the transition zone. Thus, we infer there is no resolvable net accumulation of seismic moment along the ETS portion of the plate interface averaged over the >50 year interval of the tidal and leveling data. Small earthquakes like those observed in 2004 may be a mechanism for the partial release of strain at the downdip edge of the transition zone. In contrast, much of the ETS slip and the 2004 earthquakes lie within the broad transition zones inferred from locking models constrained by horizontal GPS velocities [*Wang et al.*, 2003; *McCaffrey et al.*, 2007]. In this latter case, the ETS phenomenon and smaller earthquakes may represent the process through which partial slip is accommodated in the transition zone, and that these areas are contributing to the net accumulation of elastic strain to be released in future great earthquakes. The GPS data set is currently too limited to definitively answer the question of net moment release rate of ETS, but the vertical data may

suggest that when longer time intervals are considered, there is essentially no net strain accumulation in the area of ETS.

[45] The magnitude of coseismic subsidence and extent of rupture in past earthquakes inferred from onshore paleoseismology are generally consistent with the patterns of uplift rate and interseismic locking we have determined for the Oregon coast. The general inverse pattern of coseismic subsidence and interseismic uplift observed at the Nankai margin in Japan offers a consistency test between observations of paleoseismic subsidence and contemporary interseismic uplift at Cascadia [*Hyndman and Wang*, 1995; *Leonard et al.*, 2004]. Compilation of subsidence estimates for the 1700 event show a trend along the Oregon coast with a minimum in the South Beach area (although subsidence is observed), increasing northward to greater values along the Columbia River. South from the central Oregon minimum, mean subsidence estimates increase to greater values in the vicinity of Coos Bay (Charleston) and Cape Blanco [*Leonard et al.*, 2004]. The low, but positive interseismic uplift rates we observe along the central Oregon coast resolve the mismatch between previous estimates of interseismic subsidence and paleoseismic signs of coseismic subsidence in this area [*Mitchell et al.*, 1994; *Verdonck*, 2006].

[46] The geodetic data of our study cannot predict future coseismic behavior, but the correlation of the abrupt change in locking with paleoseismic evidence for possible rupture segmentation suggest that the geologic transitions associated with the southern end of the Siletzia block are significant for both interseismic and coseismic behavior of the Cascadia megathrust. The sharp change in locking north of Cape Blanco occurs at approximately the same latitude as the change in recurrence interval from a compilation of onshore paleoseismic studies [*Nelson et al.*, 2006]. In the Coos Bay area and north, dates of paleoearthquakes are consistent with long ruptures like the 1700 event, which spanned most of the plate boundary. To the south, there appear to be more frequent recognized earthquakes, suggesting some events may be confined to a southern Cascadia segment [*Nelson et al.*, 2006].

7. Conclusions

[47] The updated tide gauge and leveling-derived uplift rate field we have calculated provides the best estimate to date of vertical deformation along the central Cascadia margin for the past 80 years. We have identified and corrected the most significant problems in the raw leveling and tidal data that have biased previous studies. Variations in uplift rate alongstrike require significant variations in locking on the subduction interface along the Oregon margin. The pattern of locked and transition zone variation follows the extent of the mafic Siletzia block. The southern change coincides with the termination of Siletzia against the Klamath terranes. The northern change is also correlated with a pronounced structural change in the accretionary wedge that may suggest an alongstrike change in conditions along the plate interface. In contrast to some recent horizontally constrained models of Cascadia, our locking model predicts that most of the transient slip in ETS events occurs downdip from where significant net interseismic slip deficit is accumulating.

[48] Our data provide a baseline of central Cascadia vertical deformation at 598 points averaged over the late 20th century. Future geodetic measurements of vertical deformation rates may be compared to our results as we proceed later in the Cascadia seismic cycle. At this point the data do not allow for the analysis of time-dependent variations in uplift rate and subduction processes that undoubtedly exist. As the network of permanent GPS receivers along the Cascadia fore arc densifies with the Plate Boundary Observatory, and the interval over which measurements are made lengthens, there will be points with continuously recorded uplift measurements to compare with the historical uplift rates. In the near future, reoccupation of leveling bench marks and tide gauges that have not been measured since the early 20th century has the potential to yield valuable constraints for areas currently without data.

Appendix A: Sea Level Data and Processing

[49] We analyzed the stability of bench marks at the tide gauges for the periods of continuous data collection to verify the accuracy of the sea level data. Leveling ties between a tide gauge and a primary bench mark (PBM) onshore maintain a local vertical reference frame through time. There is a network of additional tidal bench marks at each tide gauge that provides redundancy and enables verification of the consistency of relative bench mark elevations. If the PBM is moving relative to a stable local reference, the water levels tied to that bench mark through the tide gauge will contain a spurious trend contributed by the local instability. Given the precision of high-quality leveling around the short loops of tide gauge bench marks and the decades over which the measurements are made, we are generally able to detect instabilities at rates >0.1 mm a^{-1}. Through this analysis, we have identified a reference tidal bench mark for each tide gauge locality which was included in the regional NGS releveling and appears to be stable in both the local and regional leveling. We have determined time-averaged rates of movement of the primary bench marks relative to these regional reference monuments for the continuous history of each gauge (Table A1). We apply linear correction rates to each sea level time series for the appropriate periods to adjust the vertical reference frame to match the vertical velocity of the regional connecting bench mark. This means that even if the reference bench mark is locally unstable at a low rate, its instability will not bias the calculated uplift rates along releveled lines that are adjusted to the tidal rate through that bench mark.

[50] Most of the studied primary bench marks settle at rates ≤ 0.2 mm a^{-1} compared to apparently stable local datums (Table A1). However, a significant problem occurred at South Beach 1967 to 1996, where the PBM settled at an initial rate of 5 mm a^{-1} for $\sim$5 years and slowed to 2 mm a^{-1} for the remainder of its time as the local reference monument (Figure A1). The other example of rapid instability comes from the Astoria gauge. Tidal 1 (1925), the PBM at Astoria for the first half of its record, was mounted in the side of a building and rose relative to stable monuments at a fairly steady rate of 1.6 mm a^{-1} (Figure A2). Previous analyses of these sea level records are biased by apparent sea level rise which was too fast at South Beach and too slow at Astoria.

[51] We exclude water level data from our analysis for periods where the data are clearly contaminated by an error not correctable using the tidal leveling data. Astoria's

Table A1. Stability of Tidal Bench Marks and Attachment to Regional NGS Leveling

Tide Gauge	Regional Attachment Bench Mark	Attachment Error (σ_r) (mm a^{-1})	Date	Primary Bench Mark	Correction Rate (mm a^{-1})
Astoria (As)	tidal 7 1939	0.3[a]	Feb 1925 to Jan 1962	tidal 1 1925	−1.60 ± 0.06
			Feb 1962 to Dec 2006	tidal 11 1959	0.18 ± 0.05
Garibaldi (Ga)	6 1927	0.3	Sep 1926 to Dec 1926	1 1926	0.00 ± 0.30
			Apr 1927 to Sep 1957	6 1927	0.00 ± 0.30
			Jun 1970 to Feb 1981	tidal 10 1970	0.00 ± 0.30
			Aug 2005 to Dec 2006	7540 A 1978	0.00 ± 0.30
South Beach (SB)	Y1	0.3	May 1928 to Mar 1934	2 1914	0.00 ± 0.30
			Feb 1967 to Jul 1972	A590 1965	4.99 ± 0.24
			Aug 1972 to Aug 1996	A590 1965	1.59 ± 0.07
			Sep 1996 to Dec 2006	C 590 1965	0.00 ± 0.10
Charleston (Ch)	tidal 1 and 3 (1928)	0.2	Apr 1933 to Mar 1934	tidal 1 and 3 (1928)	0.00 ± 0.20
			Apr 1970 to Jan 1983	tidal 7 1970	0.20 ± 0.20
			Feb 1983 to Dec 2006	2780 A 1981	0.20 ± 0.20
Port Orford (PO)	6/1937	0.1	Jul 1925 to Apr 1934	1/1924	0.05 ± 0.10
			Oct 1977 to Dec 2006	6/1937	0.00 ± 0.10
Crescent City (CC)	T 23	0.1	Jan 1933 to Apr 1933	2/1928	0.05 ± 0.10
			May 1933 to Apr 1974	6/1933	0.09 ± 0.10
			May 1974 to Dec 2006	tidal 20 reset	0.00 ± 0.10

[a]Corrections to As water level time series are well constrained by local leveling at tide gauge site, but the lack of 1930s leveling to the tide gauge site introduces additional error.

monthly mean water levels for the year of June 1948 to May 1949 are offset ∼19 cm higher than the rest of the time series as shown in differences with the nearest operating tide gauges at Crescent City, California, and Neah Bay, Washington (Figure 1). Not knowing the cause or the precise value of this offset, we exclude this year of data from the Astoria time series. We also exclude many of the data in the Garibaldi time series, as the 1970 to 1981 occupation shows a slope that is inconsistent with the long trend anchored by observations earlier in the century and the recent 1.5 years of data. Over the 1970 to 1981 period, water level at Garibaldi (Ga) appeared to fall at an anomalously high rate, which may have been caused by the float in the gauge slowly sinking with respect to the water

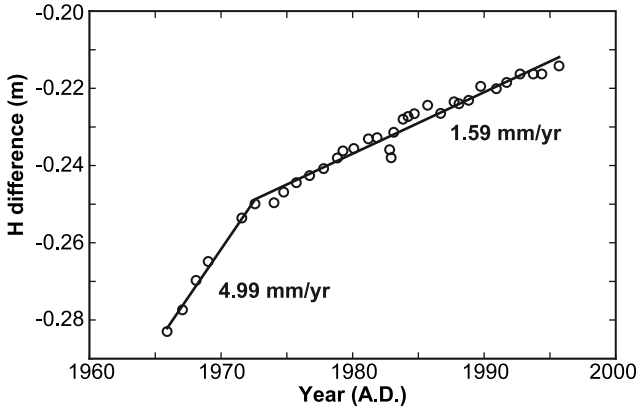

Figure A1. Time series of elevation difference of South Beach primary bench marks from local tidal leveling. Elevation difference calculated as height of bench mark C 590 minus the height of bench mark A 590. Positive slope indicates that A 590, which lies on young sediment, was settling relative to C 590. Differencing these bench marks from others in the tidal loop shows that A 590 subsided relative to its neighbors, while C 590 shows little relative motion. Leveling ties to the bench marks on the Highway 101 bridge over the Yaquina River, which has footings on bedrock, indicate that C 590 is stable with respect to bench mark Y 1, which has been releveled in the NGS regional campaigns and appears stable relative to other monuments in the Newport area. We correct the February 1967 to August 1996 portion of the South Beach tidal time series when A 590 was the primary bench mark using the slopes from the two regression lines shown fit to the data above.

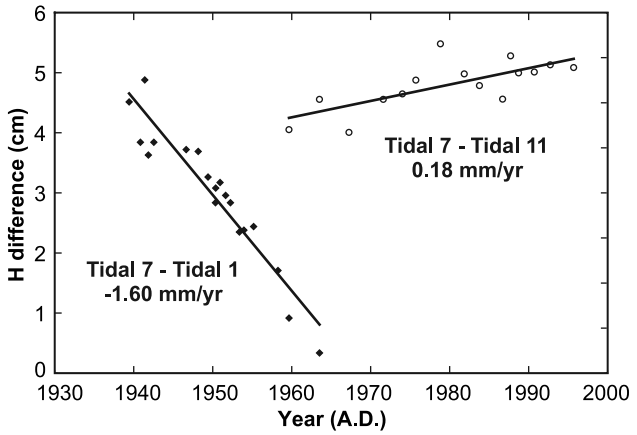

Figure A2. Time series of relative movement of tidal bench marks at the Astoria gauge from local leveling. The elevations of the two primary tidal bench marks, tidal 1 and tidal 11, are differenced from tidal 7, the bench mark we use to attach the tidal uplift rate to the regional releveling data. The negative slope of the tidal 1 time series reflects its rise relative to tidal 7. Tidal 1 was set in the side of a building which appeared to be tilting. The current NOS primary bench mark, tidal 11, appears more stable, although it dropped slightly with respect to tidal 7 over the period of these measurements. The water level record of the Astoria gauge is corrected to the reference frame of tidal 7 using the linear fits above. The behavior of tidal 1 is extreme, but differential movement similar to tidal 11 is seen at most of the tide gauges.

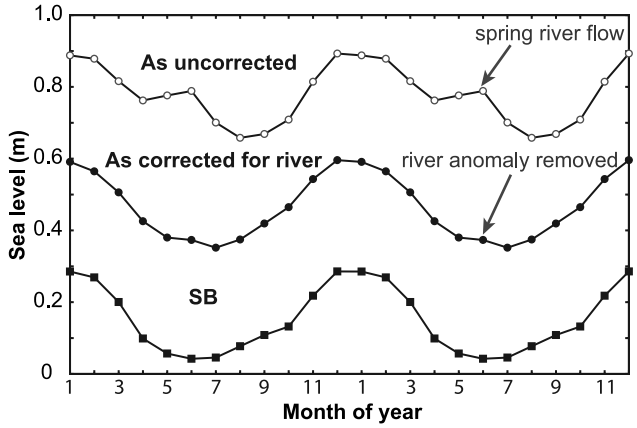

Figure A3. Mean seasonal cycles for Astoria and South Beach tide gauges plotted for two years. Uncorrected Astoria cycle diverges from the regional pattern due to high levels of Columbia River discharge in late spring and early summer [*Mitchell et al.*, 1994]. Correcting the monthly water level time series for the discharge history of the Columbia River using the relationship of Figure A5 results in a mean seasonal cycle with only a small anomaly compared to the pattern from South Beach to the south.

surface, a common problem with poorly maintained float-type gauges (B. Douglas, personal communication, 2002). The anomalous trend is most visible in differences with the time series of the nearest tide gauges, South Beach (SB) and Astoria (As) (e.g., Figure 2b). For the 1970 to 1981 interval, residuals from linear regression of the long As-Ga and SB-Ga differenced time series have slopes of 4.0 ± 1.2 mm a^{-1} and 6.0 ± 1.1 mm a^{-1}, respectively. As the trends of sea level time series of only a decade are strongly affected by oceanographic noise, we used the SB-As record to assess how unusual such trends are in residual time series. As SB and As are more widely separated than either site from Ga, the SB-As differenced time series represents a conservative estimate for the magnitude of the residual trend that should be present in the differenced time series of Ga and either site. We calculated the slopes of the possible subsets of the SB-As residual time series with the same 10.7 year length as the Ga occupation. The observed slopes in the residuals for As-Ga and SB-Ga both fall outside of the 95% prediction interval based on this analysis, and SB-Ga lies outside of the 99% prediction interval. Following the interpretation of the gauge float not maintaining a constant level, we assume that the 1970 Garibaldi tide gauge was properly installed, calibrated, and leveled to the tidal bench marks. As there is no obvious discrete step in the record, we conclude the float instability accumulated slowly during the tidal occupation, and the earliest measurements accurately reflect a long-term tidal datum. Thus, we use the first year of the Ga 1970 occupation as little to no error accumulated during that period.

[52] Much of the annual variation in a Cascadia time series of monthly mean water level is caused by seasonal variations in atmospheric pressure, the position of currents, and wind stress [*Enfield and Allen*, 1980]. Especially for sites with short or incomplete records, the position of observed data within this annual cycle affects the value of the trend calculated for the time series. The annual cycle also makes the time series highly autocorrelated, and causes greater uncertainty in the long trend. Following *Mitchell et al.* [1994], we calculate a mean annual cycle for each site (Figure A3). From each observed monthly mean value we subtract the corresponding value in the mean annual cycle (Figure A4).

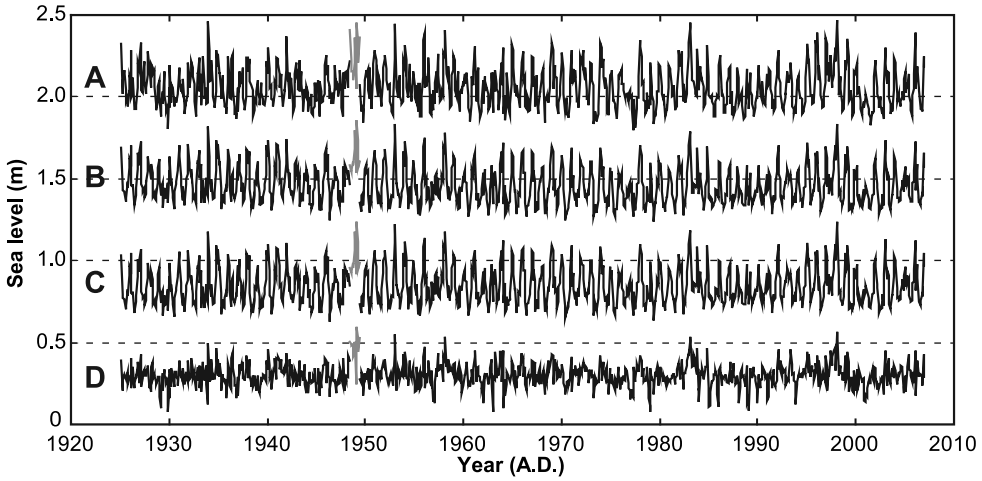

Figure A4. Sea level time series collected at Astoria tide gauge progressively processed. Gray data are year 1948–1949 that is anomalously high, and we exclude these data from the analysis. Curve A, raw time series. Curve B, corrected for water level response due to discharge rate in the Columbia River (Figure A5). Note how seasonal oceanographic cycle becomes more pronounced. Curve C, corrected for instabilities in primary bench marks relative to tidal 7, which we use to attach to regional leveling rates (Figure A2). Curve D, after removal of the mean seasonal oceanographic cycle (Figure A3). Record is much less autocorrelated, and deviations from the mean are dominated by regional oceanographic events, particularly El Niño–Southern Oscillation (the 1983 and 1998 events were particularly strong).

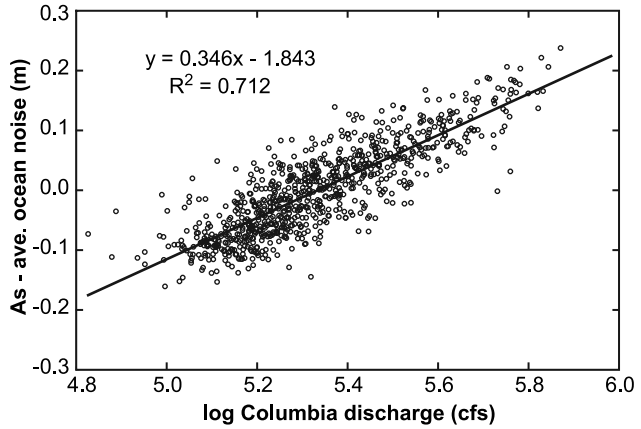

Figure A5. Response of water level measured at Astoria tide gauge to discharge in Columbia River. At high rates of discharge, the mean water level at Astoria is elevated relative to tide gauges not associated with large rivers. The slope of the regression relationship above is used to remove an averaged river effect on the tidal time series. This minimizes potential biases caused by natural and human-caused variations in river discharge through time.

[53] For the Astoria record we remove the influence of river discharge in addition to the annual cycle correction. The Astoria tidal gauge is located in the mouth of the Columbia River estuary, and its mean annual cycle diverges from the regional pattern (Figure A3) [*Mitchell et al.*, 1994]. We constructed a time series of monthly mean Columbia River discharge that spans the 1925 to 2006 Astoria tidal observations. Observations of Columbia River flow downstream of major confluences have been made intermittently by the U.S. Geological Survey near Quincy, Oregon, and we used these data to calibrate a proxy record combining the complete monthly data sets from the Willamette River at Salem, Oregon and the Columbia River at The Dalles, Oregon (Figure 1). We made a record of average ocean noise for the Cascadia outer coast by taking the mean of the residuals from the long linear trends calculated for Crescent City, California, and Neah Bay, Washington, which are located approximately equal distances north and south (Figure 1). After removing this regional oceanographic component of the variability in the Astoria record, the Columbia River effect is clear (Figure A5). We removed this calculated response of the Astoria mean water level to river flow, and then determined the mean annual cycle for Astoria using the river-corrected values. The river-corrected annual cycle for Astoria behaves similarly to nearby sites (Figure A3).

Appendix B: Uncertainty of Relative Sea Level Trends

[54] Although standard linear regression accurately estimates the linear trend of each record, sea level time series violate the assumption that successive data are unrelated to one another. Autocorrelation of residual values from linear regression means that the number of independent observations is less than the total number of monthly values in a record. Thus, the standard error of the slope, as calculated by the linear least squares method, underestimates the uncertainty of the sea level trend [*Douglas*, 2001; *Zervas*, 2001]. Removing the mean annual cycle from each record reduces the degree of autocorrelation, but the seasonally corrected time series are still affected by El Niño–Southern Oscillation signals and other regional oceanographic noise with periods greater than one year. To more accurately determine the uncertainty of the Cascadia sea level trends we apply the Hildreth-Lu procedure to account for first-order autocorrelation. The Hildreth-Lu formulation treats the value H for each month i in the time series as a function of the previous value:

$$H_i = \rho H_{i-1} + a(1-\rho) + b(t_i - \rho t_{i-1}) + \xi_i, \qquad \text{(B1)}$$

where t is time, a and b are the intercept and slope of the best fit line, ρ is the first-order autoregressive parameter describing the degree of autocorrelation, and ξ is a random, stationary time series of the nonpredictable portion of the residuals for each H_i [*Neter et al.*, 1990]. As equation (B1) is nonlinear in its parameters, we use nonlinear least squares regression to calculate a, b, and ρ for each time series. Estimates of the standard errors of the parameters are calculated analogously to the procedure for linear least squares.

[55] The sea level time series for the six southern Cascadia sites show a significant degree of autocorrelation, with values of ρ ranging of 0.27 to 0.52 for time series that do not involve the shortened Ga record that has few successive monthly values (Table 1). Accounting for the effect of autocorrelation shows that linear regression underestimates the standard error of the slope by 19% to 49%. The estimates of slope for the best fit line from the Hildreth-Lu procedure are indistinguishable from those obtained with least squares linear regression for time series with complete records. However, as the Hildreth-Lu procedure only uses data that are immediately preceded by another observation to calculate the best fit parameters, time series with many gaps will have sea level trends that do not reflect the total data set. Thus, we use the standard linear regression slope for the best estimate of the rate of change of sea level at each site, and the estimated uncertainty is obtained from the Hildreth-Lu procedure for the corresponding standard error.

Appendix C: Leveling Data Processing and Quality Assessment

[56] Within each coastal segment between tide gauges, we calculate uplift rates relative to a single common bench mark in the segment for all combinations of leveling epochs with differences greater than 5 years. This control bench mark is selected on the basis of the apparent stability of the monument through time inferred from consistent uplift rates spanning many leveling epochs and its inclusion in as many of the leveling lines for the segment as possible. Stability of the control monument makes uplift rates calculated from different combinations of leveling epochs more consistent with one another for other bench marks. We use the mean date of the survey period for each leveling line to calculate the elapsed time for uplift rates.

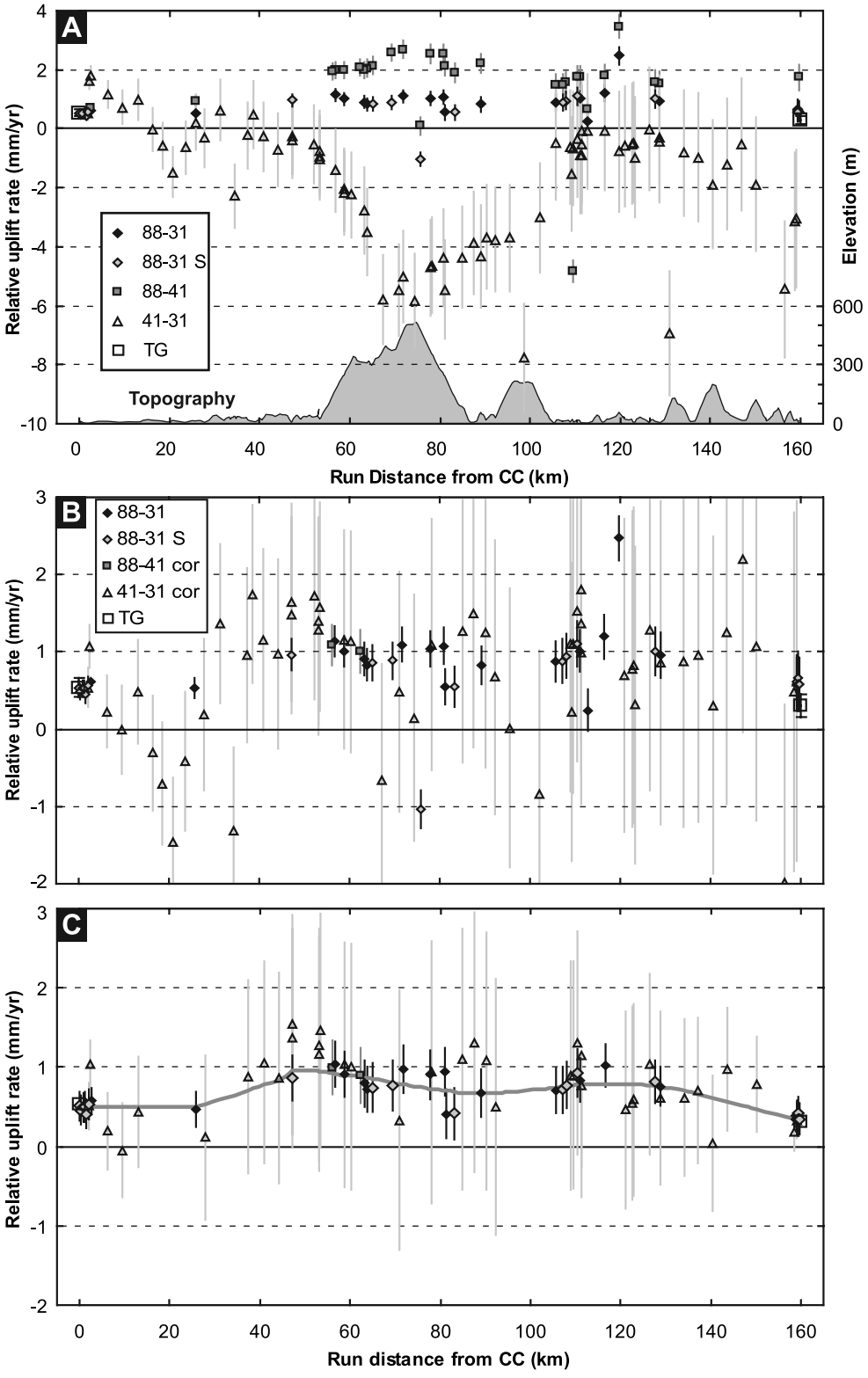
A
B
C
88-31
88-31 S
88-41
41-31
TG
88-41 cor
41-31 cor
Topography
Relative uplift rate (mm/yr)
Elevation (m)
Run Distance from CC (km)
Run distance from CC (km)

Figure C1

[57] Examination of uplift rates for each coastal segment shows that uplift rates calculated over intervals shorter than 40 years are dominated by surveying error (Figure C1a). These apparent variations in uplift rate include local excursions from the longer interval rates of up to 5 mm a^{-1} over run distances of less than 15 km. Although the short duration uplift rates do not provide meaningful data for crustal deformation, they allow insight into the timing of the most significant errors of the early leveling campaigns. Nearly all of the short-wavelength excursions in uplift rate for the 1941–1930s rates are mirrored by smaller excursions of the opposite sign for the 1980s–1941 rates, while the spatial trends of the 1980s–1930s rates are unaffected (Figure C1a). The ratios of the magnitudes of the 1941–1930s versus 1980s–1941 deviations are approximately equal to the ratios of the corresponding time intervals, suggesting that nearly all of the error for these short-wavelength features resides in the 1941 surveying. This is corroborated by the large misclosures for loops involving the 1941 coastal surveying [*Mitchell et al.*, 1994]. Additionally, line-averaged distance-dependent errors calculated by NGS from forward and backward running of segments of the same lines are greater for the 1941 lines than for any 1930s or 1980s lines.

[58] In addition to the deviations that occur on the scale of 10 km, the 1941–1930s rates show a much longer wavelength systematic northward decrease in apparent uplift rate. Relative to Crescent City, the 1941–1930s rates would result in northern Oregon subsiding at rates of 12 to 17 mm a^{-1} [*Mitchell et al.*, 1994]. This variation is clearly due to uncorrected systematic leveling error. The source of this long-wavelength systematic error is more difficult to assess than the 10-km-scale errors, but the demonstrable problems of the 1941 leveling described above suggest the long-wavelength surveying error occurred in 1941 as well. The 1980s–1930s leveling rates between tide gauges match the tidally determined relative uplift rates better than the 1980s–1941 rates. Furthermore, the signs of the discrepancies between the tidal uplift rates and the 1980s–1941 leveling are consistent with the 1980s–1941 rates being biased by an apparent northward up tilt. This apparent tilt is consistent with the cause of the observed northward down bias of the 1941–1930s rates being concentrated in the 1941 lines. These lines of evidence lead us to conclude that rates calculated using the 1941 leveling are biased by systematic errors and the 1930s leveling provides the best estimate of early 20th century elevations in western Oregon.

[59] Tidal and leveling estimates of relative uplift rates between successive pairs of tide gauges along the coast generally agree well with each other for the Oregon coast (Table 2). With the exception of the Ch-SB segment, all of the discrepancies are less than two standard errors from zero when random surveying error, uncertainty in adjusted tidal rates, and the likely error in attachment of regional leveling to the tide gauges are considered. The mismatch between the tidal and leveling rates for the Ch-SB segment is 4.5 times greater than the estimated standard error, and suggests that major systematic leveling error is present in this section. This large north-down gradient in uplift rate in the 1980s–1930s differences is largely responsible for the long-wavelength tidal-leveling mismatch that has been addressed by applying linear corrections over the entire CC to As leveling profile in previous studies [*Mitchell et al.*, 1994; *Hyndman and Wang*, 1995]. The three coastal leveling epochs again allow us to determine the likely source of the leveling error. Over the Ch-SB interval, the 1941–1930s rates show a similar north-down gradient, consistent with the regional pattern of the 1941 elevations being biased down to the north. The 1980s–1941 rates for the Ch-SB segment also yield a large north-down uplift rate gradient, with a Ch-SB leveling-tidal discrepancy of 2.08 mm a^{-1}. As discussed above, the regional systematic

Figure C1. Example of leveling data processing using the Crescent City (CC) to Port Orford (PO) coastal segment. (a) Leveling uplift rates are shown for three possible epochs of leveling differences. Secondary rates are calculated where possible to increase the number of precise 1988–1931 uplift rates (gray triangles). Bench mark uplift rates are calculated relative to the tidal uplift rate at the CC tide gauge without accounting for the regional rate of eustatic sea level rise, which would shift all data upward by 2.3 mm a^{-1} and uniformly increase the uncertainties. Error bars are propagated from the relative tidal uplift rate at Crescent City and increase proportional to $D^{1/2}$. Note that the shortest interval differences (1941–1931) show the greatest variation in apparent uplift rate, which almost certainly stems from surveying error in the 1941 survey. This inference is supported by the spatial correlation of the negative uplift rate excursion in the 1941–1931 rates with the large hill traversed by the leveling route. The 1988–1941 rates show a positive excursion in the same area, although smaller in magnitude due to the greater time over which the rates are averaged. Note the excellent agreement between the tidal and 1988–1931 leveling rates for the relative uplift rates of CC and PO. The mismatch between the other two epochs at the PO end of the line reflects the regional systematic error in the 1941 line. (b) Leveling uplift rates after correction of error in 1941 leveling. Note change in scale from Figure C1a. The correction is made assuming all of the difference in uplift rates for each bench mark that was surveyed in all three epochs is due to surveying error in 1941. For bench marks that were not surveyed in all three epochs, the error in the 1941 leveling is estimated using linear interpolation in run distance along the route, between the two nearest surrounding monuments leveled in all of the surveys. This procedure largely removes the systematic errors associated with the 1941 surveying. However, where there are few bench marks with 1988–1931 differences, systematic short-wavelength errors still exist in the 1941–1931 rates, such as near 20 km from CC. (c) Leveling data after adjustment to the relative tidal rates at both ends of the segment. Compare to Figure C1b to see how data have been shifted to better match the tidal rates (this is easiest to notice at the ends). The errors now grow inward from both ends to account for random leveling error not corrected by the segment-long adjustment. Bench marks with uplift rates that diverge from the generalized uplift rate behavior at a level that is extremely unlikely to be the result of leveling error are identified using robust, weighted loess local regression (heavy gray line). Compare with Figure C1b to see the effect of removing the outlying points. The removed bench marks with 1941–1931 rates primarily reflect incomplete correction of the 1941 leveling error. The three removed bench marks with 1988–1931 rates are contaminated by local bench mark instability at high levels.

error in the 1941 survey gives the 1980s–1941 rates a north-up bias, and the slightly better agreement of the 1980s–1941 rates is caused by this unrelated error. As both differences involving the 1988 line show the anomalous leveling uplift rate gradient, the systematic leveling error in this segment must have occurred in 1988. Since the 1980s project was a releveling of previous lines, first-order, class II survey standards allowed it to be largely single run [*Federal Geodetic Control Committee*, 1984]. Generally, the 1980s leveling appears to have been quite precise; however, systematic error may have gone unrecognized owing to only 15% of the total distance of this 1988 line being double run. Additionally, loop misclosure of 1980s leveling that includes this coastal segment is greater than would be expected for random leveling error [*Mitchell et al.*, 1994].

[60] The source of the north-down bias of the 1988 leveling between Ch and SB is difficult to identify and correct in a manner consistent with the location and style of the error accumulation. The $\sim$2 mm a^{-1} discrepancy is too large to be explained by a single blunder, as there is an anomalously high north-down uplift rate gradient over much of the segment. To correct the Ch-SB uplift rate profile we minimize the component of the velocity gradient parallel to the local strike of the subducting slab where the geometry of the leveling route permits comparison of along-strike locations. The overall path of the leveling route moves downdip above the subducting slab from Ch to SB (Figure 1). However, there are two pairs of locations in the vicinity of Reedsport where north-south separated monuments are equidistant from the -20 km slab contour [*McCrory et al.*, 2004]. We apply corrections linear with run distance to make the strike-parallel bench marks have equal uplift rates. These two combined corrections diminish the total discrepancy by 1.25 mm a^{-1}. Following these corrections a steep gradient remains at 44.2°N. Using clumps of 8 to 10 points on either side of this high gradient area to avoid bias from random scatter in the leveling data, the mean difference is 0.53 mm a^{-1} over 4.2 km of run distance and 0.7 km of downdip distance. The maximum downdip velocity gradient we observe with a smooth spline fit to east-west profiles from the Charleston and Astoria areas is 0.14 mm a^{-1} km^{-1}, so we conclude this remaining step is the result of leveling error. We make a third correction linear with run distance which reduces the step in velocity to 0.10 mm a^{-1}, conservatively allowing for a similar gradient in this area. The corrections reduce the Ch-SB leveling uplift difference by 1.68 mm a^{-1}, bringing the leveling-tidal discrepancy to 1.3 times the estimated standard error (Table 2). As these corrections are speculative, we increase the estimated errors in the modified sections to include the preadjustment relative rates.

Appendix D: Secondary Ties and 1941 Correction

[61] The tidal secondary ties take advantage of leveling conducted by the NOS at the six primary tidal sites as well as many more short-duration tide gauges along the coast. Bench marks were installed at each of these sites and were repeatedly surveyed in small leveling loops to provide vertical control for the tide gauges. As many of these subsidiary tidal sites were occupied in the 1920s and 1930s, there are records of relative bench mark elevations from the same period as the 1930–1934 regional leveling. The regional NGS leveling lines generally included at least one or two bench marks at each tidal site, but not the entire loop. In cases where one tidal bench mark was leveled in the 1930s and a different one included in the 1980s, we use the local tidal leveling from the nearest epoch to determine the relative elevations between a monument that was surveyed in the 1930s regional line and the bench mark that would be surveyed in the 1980s. These tidal secondary ties assume only that there is a negligible tectonic gradient across the $\sim$1 km dimension of the tidal loop, and that there is little survey error in the short distance tidal leveling. We add in quadrature an additional 0.1 mm a^{-1} of uncertainty to account for the likely level at which these assumptions may not hold true.

[62] Although the majority of destroyed bench marks are lost without ties to neighboring bench marks, in some cases, a replacement bench mark is monumented prior to the removal of an older bench mark. This allows a short survey with negligible error to tie between the bench marks and establish the elevation of the reset bench mark. We do not have access to the raw leveling data that have made such ties, so we download the published adjusted NAVD88 elevations from the NGS for the original and reset bench marks. The proximity of the two bench marks means that position-dependent adjustments of the raw leveling elevations are the same for the two monuments. We use the difference in adjusted elevations to establish the elevation of the reset mark in the reference frame of the 1930s regional leveling line.

[63] We have made the majority of the secondary ties by using the 1941 regional leveling to establish elevations of bench marks that were absent or not surveyed in the 1930s. This approach requires a bench mark that was surveyed in both the 1980s and 1941 and a nearby bench mark that was leveled in both the 1930s and 1941. As there are many more bench marks with 1941–1930s differences, it is generally possible to find a 1941–1930s bench mark within $\sim$1 km of any bench mark with only a 1980s–1941 difference. Although the 1941 first-order leveling contains systematic errors over long distances (discussed above), it provides relative elevations with an uncertainty of $<$2 mm over a 1 km distance. By assuming the relative elevation of the two bench marks as measured in 1941 is the same as if they had both been surveyed in the 1930s, we can calculate the elevation of the 1980s–1941 bench mark in the vertical reference frame of the 1930s line. This approach assumes that there is minimal differential uplift resulting from tectonic deformation expressed over 1 km in a decade and that the 1941–1930s bench mark did not experience local instability during the 1941–1930s period.

[64] Although the 1941–1930s uplift rates are contaminated by systematic leveling errors, the greater number of repeats for this epoch provides greater spatial density than the differences involving the 1980s leveling so we attempt to correct them using the more sparse 1980s–1930s rates to fill gaps in coverage. We calculate corrections to make the 1941–1930s rates match the 1980s–1930s rates at bench marks that were measured in all three leveling epochs. As both systematic and random leveling errors accumulate in an autocorrelated manner along the length of a leveling line, we use linear interpolation between the points where the 1941 correction is calculated to obtain corrections for 1941–

1930s rates for 334 bench marks in the gaps between 1980s and 1930s rates. Although the corrected 1941–1930s rates are strongly controlled by the pattern of 1980s–1930s uplift rates and contain greater scatter, they provide some information on the uplift rate pattern in areas that are otherwise unconstrained (Figure C1b).

Appendix E: Adjustment of Leveling Data to Tidal Rates

[65] We attach the leveling-derived uplift rates to the relative uplift rates of the tide gauges that form the segment endpoints with an uncertainty-weighted adjustment (Figure C1c). In the tidal reference frame, the uplift rate of each coastal bench mark can be estimated by the leveling that connects it to the tide gauge at either end of the segment in which it is located. From an end of a coastal segment (tide gauge "i"), the uncertainty in uplift rate of each bench mark depends on the error of the tidal uplift rate ($\sigma_{tg(i)}$), the potential uplift rate mismatch between the water level time series and the local reference bench mark ($\sigma_{r(i)}$), and the random leveling error accumulated from the reference bench mark($\sigma_{l(i)}$). The error of the tidal uplift rate, $\sigma_{tg(i)}$, is obtained through the regional adjustment of relative sea level change rates (Table 1). For $\sigma_{r(i)}$, we estimate the potential error in our corrections of the primary bench mark-based water level time series to stable-appearing reference bench marks in the regional leveling. The estimated values of $\sigma_{r(i)}$ reflect the amount and consistency of leveling ties between the local tidal bench marks and monuments leveled in regional lines (Table A1). We calculate the predicted random leveling error contribution to uncertainty in leveling uplift rate as

$$\sigma_{l(i)} = \frac{\sqrt{\left(\beta_1^2 + \beta_2^2\right) \cdot D_i}}{t_2 - t_1}, \tag{E1}$$

where t_1 and t_2 are the times of the two differenced epochs, D_i is the run distance (km) from the reference bench mark of tide gauge i, and β_1 and β_2 (mm km$^{-1/2}$) are the estimated standard deviations of height measurements over a 1 km distance for the two epochs as reported by the NGS [*Vanicek et al.*, 1980; *Dzurisin et al.*, 2002]. We use the single-run value of β for lines that were not completely double run. For sections of the coast where the leveling of an epoch is composed of more than one line, we calculate mean values β and t, weighted by the fractions of the total gauge-to-gauge run distance represented by each line. The total propagated error of bench mark uplift rate relative to the adjusted uplift rate at tide gauge i is

$$\sigma_{t(i)} = \sqrt{\sigma_{tg(i)}^2 + \sigma_{r(i)}^2 + \sigma_{l(i)}^2} \tag{E2}$$

The leveling extending from a bench mark to the next tide gauge south is separate from the leveling connecting it to the tide gauge to its north, giving two independent estimates of the uplift rate for each point. We use a weighted mean to calculate best estimates of adjusted uplift rates for each bench mark between each pair of tide gauges. For the weight w_i associated with the uplift rate given by tide gauge i, we use $w_i = \sigma_{t(i)}^{-2}$. The discrepancies between the tidal and leveling estimates for the relative velocities of the endpoints of each coastal segment are resolved by some combination of the leveling data being shifted from the tidal rates at the segment endpoints and being effectively tilted in between (Figure C1c). This method does not assume the functional form of a correction (e.g., linear with north-south distance) to make the leveling data match tidal rates at ends of a coastal profile [cf. *Mitchell et al.*, 1994; *Hyndman and Wang*, 1995]. Although the adjustment removes error at the wavelength of the segment, the leveling uplift rates may still contain random errors which compensate one another within the segment. To account for this potential error source, we calculate a mean distance-dependent error for each bench mark, σ_t, from $\sigma_{t(north)}$ and $\sigma_{t(south)}$, weighted by D_i^{-2} (Figure C1c). For the sections of the Ch-SB segment where additional corrections were applied, we include additional uncertainty for points that changed relative velocity with respect to their neighbors (the magnitude of the correction relative to the nearest end of the corrected section).

[66] Following the adjustment of uplift rates for the coastal leveling route, we attach the lines that traverse east from Coquille, Newport, and Astoria. On the eastern ends of these routes there are no precise measurements of absolute uplift rate to provide control like the tide gauges on the coast. Consequently, for each line to the east, we add the appropriate constant to all of the bench mark uplift rates so the uplift rate of the connecting bench mark has the same value determined in the coastal adjustment. This means the relative uplift rates of bench marks in the lines east from the coast are unchanged. For the South Beach-east line we correct the 1941–1930 rates for leveling error in the 1941 surveying as described above. The Coquille-east line has only 1988–1931 rates, and the Astoria-east line has 1987, 1941, 1923, and 1920 leveling. For the Astoria-east route we preferentially use the first-order 1920 leveling over the second-order 1923 leveling. The 1941–1920 rates do not show local anomalies to suggest one epoch is particularly contaminated by systematic leveling error, so we do not make any corrections to the short duration rates along this segment. We choose the most stable-appearing bench mark at the line junctions based on consistency of rates with surrounding monuments and agreement of rates calculated with different combinations of leveling epochs. This monument is used as the control monument to calculate relative uplift rates for the bench marks along the line to the east. For the two southern spur lines we use the adjusted 1980s–1930s rates for the control monuments to shift the relative uplift rates into the regional reference frame. For the northern transect, the 1930 coastal line terminated in the town of Astoria, approximately 9 km west of the Astoria tide gauge at Tongue Point. To minimize the differences in uplift rates calculated from different epochs, the control bench mark for the Ga-As coastal segment is the stable monument closest to the Astoria tide gauge with 1920s, 1930s, 1941, and 1987 elevations. The rate of the Astoria-east control bench mark is calculated with a mean of the 1987–1920, 1987–1923, and 1987–1941 rates, weighted by the leveling uncertainty between it and the control bench mark for the Ga-As segment. This better ties the Astoria-east rates to the 1987–1930 rates from the coastal line and makes the 1987–1941 rates that tie to the As tidal rate more consistent with the 1987–1920 rates, which likely provide the best estimate of uplift rate for the line to the east. We propagate uncertainty for each bench mark in

the eastern spur lines by adding in quadrature the error of the control monument from the coastal adjustment and the distance-dependent leveling uncertainty from the control monument to each bench mark.

Appendix F: Bench Mark Stability

[67] The relatively long interval between reoccupations and dense spacing of bench marks allow us to address the effects of leveling bench mark stability over longer temporal and spatial scales than previous studies [e.g., *Wyatt*, 1989]. The majority of the uplift rate data calculated from releveling intervals greater than 20 years plot in a tight band with scatter of less than $\sim$0.5 mm a^{-1}. This scatter probably represents surveying error, short-wavelength direction changes of the leveling route across the tectonic gradient, and bench mark instability. Many of the 1941–1930s corrected rates fall outside of the dense scatter of the longer interval rates, as do a small percentage of the longer interval rates. The larger scatter of the short intervals is largely due to inaccuracies in the interpolation of 1941 error correction. Outlying data calculated from long intervals almost certainly record locally unstable bench marks, due to the high precision of leveling over short distances and the expected spatial scale of tectonic signals. We eliminate data that diverge greatly from their neighbors (9% of the total long interval rates) to avoid the influence of signals that are clearly local in nature.

[68] To identify outlying points in a systematic fashion that does not rely on assumptions such as a deformation model, we generalize the pattern of uplift rate variation along the leveling route in each coastal segment with a robust loess curve. This locally weighted regression technique makes no assumptions about the overall functional form of the relationship between the two variables and is robust to outlying data [*Cleveland et al.*, 1992]. The fit is calculated using weights of σ_t^{-2} to emphasize the higher precision points. We use a span (α) of 0.3 for all segments except for the Coquille-east ($\alpha = 0.5$), which has too few data, and the Fort Stevens spur ($\alpha = 1.0$), which is only 16 km in total length. These α values produce curves that smoothly follow the densest data (Figure C1c). We use a conservative threshold in rejecting data that are 0.7 mm a^{-1} or greater from the fitted curve. This value represents four standard errors calculated from random leveling error for the relative uplift rates of two bench marks separated by 30 km surveyed in the 1930s and 1980s. Along the coastal route, 30 km is the greatest run distance between successive bench marks that have 1980s–1930s rates, including secondary ties (the mean distance is 2.4 km). Because of the high precision of the first-order leveling, the spurious uplift rates of the eliminated points are extremely unlikely to result from surveying error. The local nature of these >0.7 mm a^{-1} anomalies is also inconsistent with strain accumulation associated with crustal faulting that would produce an uplift pattern scaled by the size of a significant fault. The only plausible explanation for such deviations in uplift rate is local monument instability.

[69] Lower levels of bench mark instability clearly affect the majority of rates in our data set that pass this filtering process. However, the difficulty in defining the true tectonic uplift rate at the 0.1 mm a^{-1} level, given leveling and bench mark errors, as well as potential variations in the tectonic uplift rate pattern, does not give us confidence to more aggressively remove suspect data. The residual signs of the removed data give some insight into the process of bench mark instability. Of the 35 bench marks with long epoch differences that we removed, 30 had anomalously low uplift rates. This observation strongly suggests that the probability distribution of bench mark instability is skewed toward subsidence. Of the five anomalously high rates, one is tidal 1 at Astoria (Figure A2) where tilting of the building into which it was set, driven by overall settling, is likely. A second monument, R 100, in Warrenton, Oregon, was reported to be tilted 15° from horizontal at the time of its releveling. Given the >45 year between surveys and the 0.7 mm a^{-1} threshold, the removed bench marks accumulated greater than 32 mm total displacement relative to the generalized behavior of their neighbors. Such long-term localized relative uplift difference of a monument is certainly possible, but we find bench mark settling under the force of gravity to be the most likely cause of major instabilities. Inclusion of the greatest outliers clearly biases the uplift rates too low. Although the data are not conclusive, the asymmetry in the farthest outlying uplift rate data suggests the mean and/or mode of the bench mark instability probability distribution may be slightly negative as well.

[70] **Acknowledgments.** This work was funded by the USGS National Earthquake Hazards Reduction Program, award 05HQGR0053. Neil White was very helpful in explaining details of their sea level reconstructions and provided us with reconstructed time series for the Cascadia region. Kelin Wang offered helpful suggestions and provided us with a preprint of recent modeling results. We thank Josh Roering for conversations about this work and comments on a version of this paper. We thank Laura Wallace and Daniel Dzurisin for constructive reviews that improved the clarity of this manuscript.

References

Adam, J., D. Klaeschen, N. Kukowski, and E. Flueh (2004), Upward delamination of Cascadia Basin sediment infill with landward frontal accretion thrusting caused by rapid glacial age material flux, *Tectonics*, *23*(3), TC3009, doi:10.1029/2002TC001475.

Almond, P., J. Roering, and T. C. Hales (2007), Using soil residence time to delineate spatial and temporal patterns of transient landscape response, *J. Geophys. Res.*, *112*, F03S17, doi:10.1029/2006JF000568.

Ando, M., and E. I. Balazs (1979), Geodetic evidence for aseismic subduction of the Juan de Fuca Plate, *J. Geophys. Res.*, *84*(B6), 3023–3028, doi:10.1029/JB084iB06p03023.

Aoki, Y., and C. H. Scholz (2003), Vertical deformation of the Japanese islands, 1996–1999, *J. Geophys. Res.*, *108*(B5), 2257, doi:10.1029/2002JB002129.

Baldwin, E. M., and P. W. Howell (1949), The Long Tom, a former tributary of the Siuslaw River, *Northwest Sci.*, *23*, 112–124.

Blakely, R. J., T. M. Brocher, and R. E. Wells (2005), Subduction-zone magnetic anomalies and implications for hydrated forearc mantle, *Geology*, *33*(6), 445–448, doi:10.1130/G21447.1.

Brudzinski, M. R., and R. M. Allen (2007), Segmentation in episodic tremor and slip all along Cascadia, *Geology*, *35*(10), 907–910, doi:10.1130/G23740A.1.

Burgette, R. J., R. J. Weldon, D. Livelybrooks, D. A. Schmidt, S. K. Alba, and B. A. Wisely (2005), Constraints on the extent of subduction zone locking along the central Oregon coast from leveling and sea level observations, *Eos Trans. AGU*, *86*(52), Fall Meet. Suppl., Abstract S51C-1017.

Church, J. A., and N. J. White (2006), A 20th century acceleration in global sea-level rise, *Geophys. Res. Lett.*, *33*, L01602, doi:10.1029/2005GL024826.

Church, J. A., N. J. White, R. Coleman, K. Lambeck, and J. X. Mitrovica (2004), Estimates of the regional distribution of sea level rise over the 1950–2000 period, *J. Clim.*, *17*(13), 2609–2625, doi:10.1175/1520-0442(2004)017<2609:EOTRDO>2.0.CO;2.

Clague, J. J. (1997), Evidence for large earthquakes at the Cascadia subduction zone, *Rev. Geophys.*, *35*(4), 439–460, doi:10.1029/97RG00222.

Clague, J. J., and T. S. James (2002), History and isostatic effects of the last ice sheet in southern British Columbia, *Quat. Sci. Rev.*, *21*(1–3), 71–87, doi:10.1016/S0277-3791(01)00070-1.

Cleveland, W. S., E. Grosse, and W. M. Shyu (1992), Local regression models, in *Statistical Models in S*, edited by J. M. Chambers and T. J. Hastie, pp. 309–376, Wadsworth and Brooks, Pacific Grove, Calif.

Douglas, B. C. (2001), Sea level change in the era of the recording tide gauge, in *Sea Level Rise: History and Consequences*, *Int. Geophys. Ser.*, vol. 75, edited by B. C. Douglas, M. S. Kearney, and S. P. Leatherman, pp. 37–64, Elsevier, New York.

Dragert, H., K. L. Wang, and T. S. James (2001), A silent slip event on the deeper Cascadia subduction interface, *Science*, *292*(5521), 1525–1528, doi:10.1126/science.1060152.

Dzurisin, D., M. P. Poland, and R. Burgmann (2002), Steady subsidence of Medicine Lake volcano, northern California, revealed by repeated leveling surveys, *J. Geophys. Res.*, *107*(B12), 2372, doi:10.1029/2001JB000893.

Enfield, D. B., and J. S. Allen (1980), On the structure and dynamics of monthly mean sea level anomalies along the Pacific coast of North and South America, *J. Phys. Oceanogr.*, *10*(4), 557–578, doi:10.1175/1520-0485(1980)010<0557:OTSADO>2.0.CO;2.

Federal Geodetic Control Committee (1984), Standards and specifications for geodetic control networks, report, Natl. Oceanic and Atmos. Admin., Rockville, Md.

Fisher, M. A., E. R. Flueh, D. W. Sholl, T. Parsons, R. E. Wells, A. Tréhu, U. ten Brink, and C. S. Weaver (1999), Geologic processes of accretion in the Cascadia subduction zone west of Washington State, *Geodynamics*, *27*, 277–288, doi:10.1016/S0264-3707(98)00001-5.

Fleming, S. W., and A. M. Tréhu (1999), Crustal structure beneath the central Oregon convergent margin from potential-field modeling: Evidence for a buried basement ridge in local contact with a seaward dipping backstop, *J. Geophys. Res.*, *104*(B9), 20,431–20,447, doi:10.1029/1999JB900159.

Flück, P., R. D. Hyndman, and K. Wang (1997), Three-dimensional dislocation model for great earthquakes of the Cascadia subduction zone, *J. Geophys. Res.*, *102*(B9), 20,539–20,550, doi:10.1029/97JB01642.

Fuller, C. W., S. D. Willet, and M. T. Brandon (2006), Formation of forearc basins and their influence on subduction zone earthquakes, *Geology*, *34*(2), 65–68, doi:10.1130/G21828.1.

Gerdom, M., A. M. Tréhu, E. R. Flueh, and D. Klaeschen (2000), The continental margin off Oregon from seismic investigations, *Tectonophysics*, *329*(1–4), 79–97, doi:10.1016/S0040-1951(00)00190-6.

Goldfinger, C., C. H. Nelson, and J. E. Johnson (2003), Holocene earthquake records from the Cascadia subduction zone and northern San Andreas Fault based on precise dating of offshore turbidites, *Annu. Rev. Earth Planet. Sci.*, *31*, 555–577, doi:10.1146/annurev.earth.31.100901.141246.

Gulick, S. P. S., A. M. Meltzer, and S. H. Clarke Jr. (1998), Seismic structure of the southern Cascadia subduction zone and accretionary prism north of the Mendocino triple junction, *J. Geophys. Res.*, *103*(B11), 27,207–27,222, doi:10.1029/98JB02526.

Gutscher, M. A., D. Klaeschen, E. Flueh, and J. Malavieille (2001), Non-Coulomb wedges, wrong-way thrusting, and natural hazards in Cascadia, *Geology*, *29*(5), 379–382, doi:10.1130/0091-7613(2001)029<0379:NCWWWT>2.0.CO;2.

Holdahl, S. R., R. Faucher, and H. Dragert (1989), Contemporary vertical crustal movement in the Pacific Northwest, in *Slow Deformation and Transmission of Stress in the Earth*, *Geophys. Monogr. Ser.*, vol. 49, edited by S. C. Cohen and P. Vanicek, pp. 17–29, AGU, Washington, D. C.

Hyndman, R. D., and K. Wang (1995), The rupture zone of Cascadia great earthquakes from current deformation and the thermal regime, *J. Geophys. Res.*, *100*(B11), 22,133–22,154, doi:10.1029/95JB01970.

Hyndman, R. D., K. Wang, T. Yuan, and G. D. Spence (1993), Tectonic sediment thickening, fluid expulsion, and the thermal regime of subduction zone accretionary prisms: The Cascadia margin off Vancouver Island, *J. Geophys. Res.*, *98*(B12), 21,865–21,876, doi:10.1029/93JB02391.

Jacoby, G. C., D. E. Bunker, and B. E. Benson (1997), Tree-ring evidence for an AD 1700 Cascadia earthquake in Washington and northern Oregon, *Geology*, *25*(11), 999–1002, doi:10.1130/0091-7613(1997)025<0999:TREFAA>2.3.CO;2.

James, T. S., J. J. Clague, K. L. Wang, and I. Hutchinson (2000), Postglacial rebound at the northern Cascadia subduction zone, *Quat. Sci. Rev.*, *19*(14–15), 1527–1541, doi:10.1016/S0277-3791(00)00076-7.

Kelsey, H. M., D. C. Engebretson, C. E. Mitchell, and R. L. Ticknor (1994), Topographic form of the Coast Ranges of the Cascadia margin in relation to coastal uplift rates and plate subduction, *J. Geophys. Res.*, *99*(B6), 12,245–12,255, doi:10.1029/93JB03236.

Kelsey, H. M., R. L. Ticknor, J. G. Bockheim, and C. E. Mitchell (1996), Quaternary upper plate deformation in coastal Oregon, *Geol. Soc. Am. Bull.*, *108*(7), 843–860, doi:10.1130/0016-7606(1996)108<0843:QUPDIC>2.3.CO;2.

Leonard, L. J., R. D. Hyndman, and S. Mazzotti (2004), Coseismic subsidence in the 1700 great Cascadia earthquake: Coastal estimates versus elastic dislocation models, *Geol. Soc. Am. Bull.*, *116*(5), 655–670, doi:10.1130/B25369.1.

Mackay, M. E., G. F. Moore, G. R. Cochrane, J. C. Moore, and L. D. Kulm (1992), Landward vergence and oblique structural trends in the Oregon margin accretionary prism: Implications and effect on fluid flow, *Earth Planet. Sci. Lett.*, *109*(3–4), 477–491, doi:10.1016/0012-821X(92)90108-8.

Mazzotti, S., A. Lambert, N. Courtier, L. Nykolaishen, and H. Dragert (2007), Crustal uplift and sea level rise in northern Cascadia from GPS, absolute gravity, and tide gauge data, *Geophys. Res. Lett.*, *34*, L15306, doi:10.1029/2007GL030283.

McCaffrey, R., M. D. Long, C. Goldfinger, P. C. Zwick, J. L. Nabelek, and C. K. Johnson (2000), Rotation and plate locking at the southern Cascadia subduction zone, *Geophys. Res. Lett.*, *27*(19), 3117–3120, doi:10.1029/2000GL011768.

McCaffrey, R., A. I. Qamar, R. W. King, R. Wells, G. Khazaradze, C. A. Williams, C. W. Stevens, J. J. Vollick, and P. C. Zwick (2007), Fault locking, block rotation and crustal deformation in the Pacific Northwest, *Geophys. J. Int.*, *169*(3), 1315–1340, doi:10.1111/j.1365-246X.2007.03371.x.

McCrory, P. A., J. L. Blair, D. H. Oppenheimer, and S. R. Walter (2004), Depth to the Juan de Fuca slab beneath the Cascadia subduction margin: A 3-D model for sorting earthquakes, *Data Ser. 91*, U.S. Geol. Surv., Reston, Va.

McNeill, L. C., C. Goldfinger, L. D. Kulm, and R. S. Yeats (2000), Tectonics of the Neogene Cascadia forearc basin: Investigations of a deformed late Miocene unconformity, *Geol. Soc. Am. Bull.*, *112*(8), 1209–1224, doi:10.1130/0016-7606(2000)112<1209:TOTNCF>2.3.CO;2.

Miller, M. M., D. J. Johnson, C. M. Rubin, H. Dragert, K. Wang, A. Qamar, and C. Goldfinger (2001), GPS-determination of along-strike variation in Cascadia margin kinematics: Implications for relative plate motion, subduction zone coupling, and permanent deformation, *Tectonics*, *20*(2), 161–176, doi:10.1029/2000TC001224.

Mitchell, C. E., P. Vincent, R. J. Weldon, and M. A. Richards (1994), Present-day vertical deformation of the Cascadia margin, Pacific Northwest, United States, *J. Geophys. Res.*, *99*(B6), 12,257–12,277, doi:10.1029/94JB00279.

Moeller, B. (1990), Stream capture in the Central Oregon Coast Range and its relationship to tectonic and structural geology, M.S. thesis, Univ. of Oreg., Eugene.

Murray, M. H., and M. Lisowski (2000), Strain accumulation along the Cascadia subduction zone, *Geophys. Res. Lett.*, *27*(22), 3631–3634, doi:10.1029/1999GL011127.

Nelson, A. R., et al. (1995), Radiocarbon evidence for extensive plate-boundary rupture about 300 years ago at the Cascadia subduction zone, *Nature*, *378*(6555), 371–374, doi:10.1038/378371a0.

Nelson, A. R., H. M. Kelsey, and R. C. Witter (2006), Great earthquakes of variable magnitude at the Cascadia subduction zone, *Quat. Res.*, *65*(3), 354–365, doi:10.1016/j.yqres.2006.02.009.

Neter, J., W. Wasserman, and M. H. Kutner (1990), *Applied Linear Statistical Models*, 3rd ed., 1181 pp., Richard D. Irwin, Homewood, Ill.

Oleskevich, D. A., R. D. Hyndman, and K. Wang (1999), The updip and down-dip limits to great subduction earthquakes: Thermal and structural models of Cascadia, south Alaska, SW Japan, and Chile, *J. Geophys. Res.*, *104*(B7), 14,965–14,992, doi:10.1029/1999JB900060.

Parsons, T., R. Wells, M. Fisher, E. Flueh, and U. ten Brink (1999), Three-dimensional velocity structure of Siletzia and other accreted terranes in the Cascadia forearc of Washington, *J. Geophys. Res.*, *104*(B8), 18,015–18,039, doi:10.1029/1999JB900106.

Personius, S. F. (1995), Late Quaternary stream incision and uplift in the forearc of the Cascadia subduction zone, western Oregon, *J. Geophys. Res.*, *100*(B10), 20,193–20,210, doi:10.1029/95JB01684.

Petersen, M. D., C. H. Cramer, and A. D. Frankel (2002), Simulations of seismic hazard for the Pacific Northwest of the United States from earthquakes associated with the Cascadia subduction zone, *Pure Appl. Geophys.*, *159*(9), 2147–2168, doi:10.1007/s00024-002-8728-5.

Reilinger, R., and J. Adams (1982), Geodetic evidence for active landward tilting of the Oregon and Washington coastal ranges, *Geophys. Res. Lett.*, *9*(4), 401–403, doi:10.1029/GL009i004p00401.

Satake, K., K. Shimazaki, Y. Tsuji, and K. Ueda (1996), Time and site of a giant earthquake in Cascadia inferred from Japanese tsunami records of January 1700, *Nature*, *379*(6562), 246–249, doi:10.1038/379246a0.

Satake, K., K. L. Wang, and B. F. Atwater (2003), Fault slip and seismic moment of the 1700 Cascadia earthquake inferred from Japanese tsunami descriptions, *J. Geophys. Res.*, *108*(B11), 2535, doi:10.1029/2003JB002521.

Savage, J. C. (1983), A dislocation model of strain accumulation and release at a subduction zone, *J. Geophys. Res.*, *88*(B6), 4984–4996, doi:10.1029/JB088iB06p04984.

Savage, J. C., M. Lisowski, and W. H. Prescott (1981), Geodetic strain measurements in Washington, *J. Geophys. Res.*, *86*(B6), 4929–4940, doi:10.1029/JB086iB06p04929.

Savage, J. C., M. Lisowski, and W. H. Prescott (1991), Strain accumulation in western Washington, *J. Geophys. Res.*, *96*(B9), 14,493–14,507, doi:10.1029/91JB01274.

Savage, J. C., J. L. Svarc, W. H. Prescott, and M. H. Murray (2000), Deformation across the forearc of the Cascadia subduction zone at Cape Blanco, Oregon, *J. Geophys. Res.*, *105*(B2), 3095–3102, doi:10.1029/1999JB900392.

Snay, R., M. Cline, W. Dillinger, R. Foote, S. Hilla, W. Kass, J. Ray, J. Rohde, G. Sella, and T. Soler (2007), Using global positioning system-derived crustal velocities to estimate rates of absolute sea level change from North American tide gauge records, *J. Geophys. Res.*, *112*, B04409, doi:10.1029/2006JB004606.

Song, T. R. A., and M. Simons (2003), Large trench-parallel gravity variations predict seismogenic behavior in subduction zones, *Science*, *301*(5633), 630–633, doi:10.1126/science.1085557.

Svarc, J. L., J. C. Savage, W. H. Prescott, and M. H. Murray (2002), Strain accumulation and rotation in western Oregon and southwestern Washington, *J. Geophys. Res.*, *107*(B5), 2087, doi:10.1029/2001JB000625.

Szeliga, W., T. Melbourne, M. Santillan, and M. Miller (2008), GPS constraints on 34 slow slip events within the Cascadia subduction zone, 1997–2005, *J. Geophys. Res.*, *113*, B04404, doi:10.1029/2007JB004948.

Thomas, A. L. (1993), Poly3d: A three-dimensional, polygonal element, displacement discontinuity boundary element computer program with applications to fractures, faults, and cavities in the Earths crust, 69 pp., Stanford Univ., Stanford, Calif.

Tréhu, A. M., I. Asudeh, T. M. Brocher, J. H. Luetgert, W. D. Mooney, J. L. Nabelek, and Y. Nakamura (1994), Crustal architecture of the Cascadia forearc, *Science*, *266*(5183), 237–243, doi:10.1126/science.266.5183.237.

Tréhu, A. M., J. Braunmiller, and J. L. Nabelek (2008), Probable low-angle thrust earthquakes on the Juan de Fuca–North America plate boundary, *Geology*, *36*(2), 127–130, doi:10.1130/G24145A.1.

Underwood, M. B. (2002), Strike-parallel variations in clay minerals and fault vergence in the Cascadia subduction zone, *Geology*, *30*(2), 155–158, doi:10.1130/0091-7613(2002)030<0155:SPVICM>2.0.CO;2.

Vanicek, P., R. O. Castle, and E. I. Balazs (1980), Geodetic leveling and its applications, *Rev. Geophys.*, *18*(2), 505–524, doi:10.1029/RG018i002p00505.

Verdonck, D. (1995), 3-Dimensional model of vertical deformation at the southern Cascadia subduction zone, western United States, *Geology*, *23*(3), 261–264, doi:10.1130/0091-7613(1995)023<0261:TDMOVD>2.3.CO;2.

Verdonck, D. (2005), An inverse dislocation model of surface deformation in western Washington, *Tectonophysics*, *395*(3–4), 179–191, doi:10.1016/j.tecto.2004.09.010.

Verdonck, D. (2006), Contemporary vertical crustal deformation in Cascadia, *Tectonophysics*, *417*(3–4), 221–230, doi:10.1016/j.tecto.2006.01.006.

Wang, K. (2007), Elastic and viscoelastic models of crustal deformation in subduction earthquake cycles, in *The Seismogenic Zone of Subduction Thrust Faults*, edited by T. Dixon and J. C. Moore, pp. 540–575, Columbia Univ. Press, New York.

Wang, K. L., and Y. Hu (2006), Accretionary prisms in subduction earthquake cycles: The theory of dynamic Coulomb wedge, *J. Geophys. Res.*, *111*, B06410, doi:10.1029/2005JB004094.

Wang, K. L., J. H. He, H. Dragert, and T. S. James (2001), Three-dimensional viscoelastic interseismic deformation model for the Cascadia subduction zone, *Earth Planets Space*, *53*(4), 295–306.

Wang, K., R. Wells, S. Mazzotti, R. D. Hyndman, and T. Sagiya (2003), A revised dislocation model of interseismic deformation of the Cascadia subduction zone, *J. Geophys. Res.*, *108*(B1), 2026, doi:10.1029/2001JB001227.

Wells, R. E., and R. W. Simpson (2001), Northward migration of the Cascadia forearc in the northwestern US and implications for subduction deformation, *Earth Planets Space*, *53*(4), 275–283.

Wells, R. E., C. S. Weaver, and R. J. Blakely (1998), Forearc migration in Cascadia and its neotectonic significance, *Geology*, *26*(8), 759–762, doi:10.1130/0091-7613(1998)026<0759:FAMICA>2.3.CO;2.

Wells, R. E., R. J. Blakely, Y. Sugiyama, D. W. Scholl, and P. A. Dinterman (2003), Basin-centered asperities in great subduction zone earthquakes: A link between slip, subsidence, and subduction erosion?, *J. Geophys. Res.*, *108*(B10), 2507, doi:10.1029/2002JB002072.

Westbrook, G. K. (1994), Growth of accretionary wedges off Vancouver Island and Oregon, *Proc. Ocean Drill. Program Initial Rep.*, 146, pp. 381–388.

Wolf, P. R., and C. D. Ghilani (1997), *Adjustment Computations: Statistics and Least Squares in Surveying and GIS*, 3rd ed., 564 pp., John Wiley, New York.

Wyatt, F. K. (1989), Displacement of surface monuments: Vertical motion, *J. Geophys. Res.*, *94*(B2), 1655–1664, doi:10.1029/JB094iB02p01655.

Yamaguchi, D. K., B. F. Atwater, D. E. Bunker, B. E. Benson, and M. S. Reid (1997), Tree-ring dating the 1700 Cascadia earthquake, *Nature*, *389*(6654), 922–923, doi:10.1038/40048.

Zervas, C. (2001), Sea level variations of the United States 1854–1999, *Tech. Rep. NOS CO-OPS 36*, 65 pp., NOAA, Silver Spring, Md.

R. J. Burgette, D. A. Schmidt, and R. J. Weldon II, Department of Geological Sciences, University of Oregon, Eugene, OR 97403-1272, USA. (rburgett@uoregon.edu)